# Towards Assessing NARCCAP Regional Climate Model Credibility for the North American Monsoon: Future Climate Simulations

Melissa S. Bukovsky[1,2], Carlos M. Carrillo[3], David J. Gochis[2], Dorit M. Hammerling[2], Rachel R. McCrary[2], Linda O. Mearns[2]

[2]National Center for Atmospheric Research, Boulder, CO

[3]University of Arizona, Tucson, AZ

Submitted to Journal of Climate

October 9, 2014



---

[1] *Corresponding author address*:
Melissa S. Bukovsky, NCAR/IMAGE, P.O. Box 3000, Boulder, CO 80307.
Email: bukovsky@ucar.edu

ABSTRACT

This study presents climate change results from the North American Regional Climate Change Assessment Program (NARCCAP) suite of dynamically downscaled simulations for the North American monsoon system in the Southwestern U.S. and Northwestern Mexico. The focus is on changes in precipitation and the processes driving the projected changes from the available regional climate simulations and their driving coupled atmosphere-ocean global climate models. The effect of known biases on the projections is also examined. Overall, there is strong ensemble agreement for a decrease in precipitation during the monsoon season; however, this agreement and the magnitude of the ensemble mean change is likely very deceiving, as the greatest decreases are produced by the simulations that are the most biased in the baseline/current climate. Furthermore, some of the greatest decreases in precipitation are being driven by changes in the large-scale that are less credible, while in some other simulations, the large-scale change may be plausible, but other biases in the simulations may be affecting the magnitude of the projected changes and driving greater precipitation decreases.

## 1. Introduction

Annual drying, increased aridity, and decreased streamflow have been projected for the Southwest U.S. (SWUS) and Northwestern Mexico (MX) due to increased greenhouse gas forcing in analyses focusing on the Coupled Model Intercomparison Project Phases 3 and 5 (CMIP3 and CMIP5, respectively) global climate model (GCM) simulations (e.g. Milly et al. 2005, Christensen et al. 2007, Hoerling and Eischeid 2007, Seager et al. 2007, Seth et al. 2013, and Cook and Seager 2013). Statements about precipitation associated specifically with the North American monsoon (NAM) season for these regions are more uncertain, however. In the CMIP3 suite of GCMs a decrease in summertime mean precipitation was projected for the SWUS and northwest MX, but model agreement on that projection was weak (Christensen et al. 2007, fig. 11.12). In the CMIP5 ensemble, decreases in monsoon season rainfall are small and insignificant, overall, given a shift in the season to less early season rainfall (June-July) and more late season rainfall (September-October) due to local and remote processes creating a more unfavorable early season convective environment (Seth et al. 2011, Cook and Seager 2013, Seth et al. 2013, and Torres-Alavez et al. 2014). The CMIP3 and CMIP5 models, however, have problems simulating precipitation in this region. During monsoon season, performance is mixed, with reasonable precipitation in some models, but a complete lack of a monsoon in others. Late monsoon season termination is a widespread and common problem also, and the annual cycle is usually too wet, particularly in winter (Lin et al. 2008, Dominguez et al. 2010, Cook and Seager 2013, Geil et al. 2013, and Torres-Alavez et al. 2014.)

Uncertainty in precipitation projections for the NAM is high partly because of the dependence of the system on dynamics and fine-scale orography that are not well-resolved by many models, particularly at typical global model scales. For example, the representation of mountains and their effects on moisture convergence has been shown to be important in projections of precipitation in this region (Gao et al. 2012). Near-surface flow and sea-surface temperatures (SSTs) over the Gulf of California (GoC) are also important and not resolved at coarse resolutions (Mitchell et al. 2002; Collier and Zhang 2007; Lee et al. 2007). Note however that higher resolution models that can resolve features like the GoC do not always produce a proficient simulation of these features either (e.g. Gutzler et al. 2009; Bukovsky et al. 2013). Geil et al. (2013) found no major differences in model performance between higher and lower resolution members in the CMIP5 ensemble for this region, where the models ranged from about 0.57º - 3.76º in resolution. In that case, even the highest resolution model was determined to be too coarse to capture smaller-scale orographically driven process. At a resolution near that of the highest resolution models in CMIP5 (50km), however, Bukovsky et al. (2013) showed that some regional models could produce some of the terrain forcing and mesoscale features important to a good representation of the NAM. Perhaps this difference is due to the use of parameterizations that are adjusted for mid-latitudes and not generalized for global use. Castro et al. (2007a), Castro et al. (2007b), and Castro et al. (2012) have also demonstrated the potential of regional models to improve forecasts of the NAM system. Therefore, in an attempt to overcome some of the uncertainty due to resolution, in this study we will present precipitation projections from the set of 50-km resolution dynamically downscaled simulations produced as a part of the North American Regional Climate Change Assessment Program (NARCCAP, Mearns et al. 2012).

This study builds off of Bukovsky et al. (2013, hereafter BUK13), where it was shown that many of the NARCCAP regional climate models (RCMs) do reasonably simulate the NAM system and its topographically influenced mesoscale features when forced with a reanalysis product, within the limits of their given resolution. However, most of the RCMs undergo a major reduction of skill when forced by GCMs in the baseline climate scenario because of the biases they inherit from the GCMs. In BUK13, some of the identified inherited biases include: atmospheric moisture content, which led to huge dry biases and no monsoon precipitation signal in some of the RCMs; SST biases, which were serendipitously favorable in the GoC; and large-scale circulation errors that, at a minimum, caused problems in the timing and magnitude of the monsoon. In the RCMs, biases related to the still too coarse resolution for many the NAM system features were also identified, and were shown to be RCM specific and not dependent on the driver. For example, while the RCMs provided a good terrain-driven spatial pattern of precipitation in the region for their resolution, not all of them were able to simulate a reasonable GoC low-level jet (LLJ), which likely contributed to those models' low precipitation biases in Arizona (AZ).

In this study, we identify further biases in the baseline climate and discuss how these biases and those presented in BUK13 may affect the projections of NAM precipitation for the future. We also identify processes responsible for the changes in precipitation projected by the RCMs. It is this deeper analysis of the simulations that then allows us to assess their differential credibility.

This paper is organized as follows: section 2 describes the NARCCAP simulations, the reanalyses used for comparison in this paper, and some of the analysis methods. Sections 3 and 4 present the results, with an analysis of the precipitation projections in section 3 and an in-depth look at what is driving those projections and how identified biases affect them in section 4. Finally, a brief summary and a discussion of the credibility of the projections are presented in section 5.

## 2. Models, methods, and datasets

### *a. Models*

Six RCMs were used to downscale four GCMs to 50-km as a part of NARCCAP. Results from 11 of the 12 planned combinations are available and included in this study. Table 1 provides an overview of the RCMs and GCMs; Table 2 presents the RCM-GCM simulation combinations. When referring to an RCM and its parent GCM, we list the forcing simulation in lower case, e.g., WRFG-ccsm; otherwise, all acronyms are in upper case.

All future simulations utilize the Special Report on Emissions Scenarios (SRES; IPCC 2000) A2 emissions scenario; the 20th-century (20c3m) emission representation is used for the baseline period. All baseline simulations span 1971-1999, while the future simulations span 2041-2069. All averages herein are performed over these specified years.

The region of NAM influence our analysis focuses on is defined in fig. 1. This also includes two specific subregions over Arizona (AZ) and northwestern Mexico (MX). Note that there is some variation in the size and placement of these regions in each model due to differences in their map projections and the southward extent of their domains. Most of the RCM domains do not extend very far south of the Baja Peninsula; thus, for some consistency, but to include as much of the domain as possible, the southern edge of the analysis region is defined to be as close to 20°N as possible. In ensemble mean plots, however, the largest common domain is used instead.

The core of the monsoon season is the target period of our analysis. We use a July-August (JA) average instead of the traditional June to August (JJA) or June to September (JJAS) average because of the challenge CMIP3 GCMs have in simulating monsoon onset and retreat (e.g. Geil et al. 2013). These GCM characteristics are transferred to some of the NARCCAP simulations, as documented in BUK13.

### *b. Verification Datasets*

Three reanalysis datasets are used briefly in model verification. They are: the National Centers for Environmental Predication's (NCEP)/Department of Energy (DOE) Reanalysis II (hereafter NCEP; Kanamitsu et al. 2002), the North American Regional Reanalysis (NARR; Mesinger et al. 2006), and the European Centre for Medium-Range Weather Forecasts (ECMWF) Reanalysis (ERA) Interim (ERA-I, Dee et al. 2011). NCEP was also used to force the NARCCAP RCM's, and is only used here in an examination of 500-hPa winds and geopotential heights. NARR was compared to several other observationally-based datasets and the NARCCAP NCEP- and GCM-forced simulations in BUK13 during the NAM season and over the same regions used herein. Its precipitation is used again in this complementary study for consistency, and because it was found that the spread in the models is considerably larger than the spread in the observationally-based datasets.

### *c. Statistical Methods*

#### 1) SIGNIFICANCE TESTING

Unless otherwise noted, statistical significance is tested at the 0.1 level using bootstrapping with bias correction and acceleration following von Storch and Zwiers (1999) and Efron and Tibshirani (1993), as described in Bukovsky and Karoly (2011).

2) ANOVA CALCULATIONS

The statistical analysis that will be presented in table 3 is done in three steps. First, we tested the hypothesis that the average rainfall, rainfall intensity, and fraction of dry days in the NARCCAP model runs have mean values equal to the corresponding NARR values using two-sided, one-sample t-tests. Secondly, we assessed whether the differences between future and baseline average rainfall, rainfall intensity and fraction of dry days in the NARCCAP model runs were zero. We used two-sided pair-wise t-tests, where a pair consists of the future and past values from the same model. Thirdly, we tested the hypotheses that the means of the differences between the baseline and future for average rainfall, rainfall intensity and the fraction of dry days differ as a function of the driving GCMs. In the case of a significant difference, we conducted a multi comparison procedure to identify which pairs are different. A multiple comparison procedure adjusts for the fact that the chance of incorrectly finding a significant difference increases with the number of comparisons when comparing individual pairs and instead provides an upper bound on the probability that any comparison will be incorrectly found significant. We conducted all analyses separately for the NAM region and the two subregions, AZ and MX.



## 3. Precipitation Projections

As illustrated in fig. 2, the 11-RCM mean projects a decrease in JA average precipitation across the region. While most of the changes in precipitation are within the bounds of natural variability in the majority of the models, there is strong agreement on the sign of the change in much of the region, particularly in Southwest AZ and northwest MX. The majority of the models agree that changes are significant and decreasing, as indicated by the hatching in fig. 2, in the central Plains and at a few locations along the west coast of Mexico and Baja Peninsula.

The ensemble mean, however, does not capture the large variability in magnitude and spatial distribution of the precipitation projections across the 11 simulations (Fig. 3). There are some broad similarities across RCMs that have the same parent GCM, but among those, one still finds substantial variation across RCMs when the details are examined. As the spatial distribution of convection in this region is governed largely by local orography, it might be expected that some of the changes would be thusly distributed, but even that is difficult to discern. The Sierra Madre Occidental (SMO) appears to influence the pattern of change in some of the RCMs (more or less precipitation on one side or the other), but this is not consistent across the models. Similarly, the Mogollon Rim in AZ appears in the pattern, but again, with no clear influence on the direction of change.

However, broadly speaking, the CCSM- and CGCM-forced simulations generally project less future precipitation for most of the region, particularly MX. In the CCSM-forced simulations, this is opposite to what the CCSM projects. This is not the only region where RCMs forced with this CCSM simulation produce precipitation projections that are contrary to what the CCSM produces, nor are these the only RCM simulations that do this (Bukovsky and Karoly 2011, Mearns et al. 2013). The other RCMs do not produce a signal that is as widespread in as consistent a manner as the CCSM- and CGCM-driven simulations.

To aid in the interpretation of these precipitation projections, we present a summary for average precipitation, precipitation intensity, and the number of dry days (DD) in table 3. The values are averaged over the NAM, AZ, and MX regions in fig. 1 only over land. The upper part shows the individual model values and the lower part both the full-model ensemble and GCM-driven sub-ensemble means. Overall, most models indicate a small increase in the number of dry days over the full region and over AZ, with a larger increase over MX. The number of dry day projections is most consistent in magnitude and sign across the full ensemble and the sub-ensembles than for other precipitation metrics, and in the full ensemble mean, this change is significantly different from zero. However, as regards the current climate simulations as a group, the number of dry days is also significantly biased relative to NARR. For mean precipitation change, it is clear here, as in fig. 3, that the CCSM- and CGCM-forced simulations produce the greatest percent decrease. The same is true for projected decreases in intensity. Examining these simulations in terms of percent decreases, however, is slightly misleading, as they are strongly dry biased to start, which is why absolute changes are given as well. However, in terms of intensity, the projections from the CGCM-driven RCMs are significantly different from the HADCM-driven RCMs in the NAM region and both the HADCM- and GFDL-driven RCMs in MX (as indicated by the underlined values in table 3). This was determined using an unbalanced one-way ANOVA (see section 2.c.2) to test if the means of the absolute differences between the current and the future in table 3 differ as a function of the driving GCMs. The differences in projections between the GCM-driven sub-ensembles are not significant for average precipitation or dry days, however.

Within the GFDL-driven group in table 3, projections are less in agreement over all regions, particularly with regard to the HRM3-gfdl and the ECP2-gfdl. The same is true, to some extent, in the two HADCM-forced simulations. The HRM3-hadcm simulates a strong percent decrease in precipitation average and intensity over AZ and an increase in the number of dry days, with a slight increase in average and intensity over MX. This is in disagreement with the MM5I-hadcm, which projects little change in AZ, and a stronger decrease in average and intensity in MX.

The change in the frequency of 3-hourly precipitation rates/events during JA is illustrated in Fig. 4 for the MX and AZ subregions. All but one of the RCM-GCM combinations simulates a decrease in the frequency of events of nearly every magnitude; the ECP2-gfdl is an outlier. The decrease in frequency is strongest in the CCSM- and CGCM-driven simulations. The decrease is smaller, though not always insignificant, in the other simulations. Several simulations indicate an increase in the frequency of events that are classified at or above the 99th percentile in the baseline period, particularly in MX in the non- CCSM- and CGCM-forced simulations. An increase in the frequency of heavy precipitation events is a common, nearly global result over land in projections of climate change, and is driven by increases in water vapor content (e.g. Solomon et al. 2007, Stocker et al. 2013)

The rainfall amplitude and frequency projections for wet and dry years only are shown in tables 4 and 5, respectively. Wet years (current or future) are defined as years that exceed a Standardized Precipitation Index (SPI, McKee et al. 1993) value of 1 and dry years as those that fall below -1 SPI. Most simulations have at least five wet and five dry years using this definition. In the 0.25 quantile, the frequency is measured as the number of days with precipitation less than or equal to the 0.25 quantile threshold, for other quantiles, the frequency is the number of days greater than or equal to the given threshold. For the full ensemble mean, tables 4 and 5 show a negative change in the amplitude of the 0.5 quantile for both wet (-15.1%) and dry (-19.4%)

years, which is consistent with results presented above. However, the more interesting results occur in the 0.99 quantile for wet years and the 0.25 quantile for dry years. In wet years, an increase in the amplitude and frequency in the 0.99 quantile is seen in the full ensemble mean, and three of the four sub-ensembles, with differences among individual simulations. For dry years, an increase in the frequency of 0.25 quantile days is seen. Both results simultaneously suggest that extreme wet years get wetter and extreme dry years get drier. Results here are also consistent with those above in that in the CCSM-driven and CGCM-driven simulations, the extreme wet years projection is damped compared to the other sub-ensembles and the extreme dry years projection is enhanced. That is, the driest biased models have drier projections.

Overall, combining these precipitation projections with the analysis of BUK13, we find that the simulations that have the greatest biases in precipitation during the monsoon season also have some of the greatest decreases in future precipitation total, intensity, and frequency. This is emphasized in fig. 5 for average JA precipitation.

## 4. Understanding the precipitation projections

In this section, we examine the processes driving the precipitation projections. The aim is to determine if the projected precipitation change is reasonable/credible, despite the known biases in the baseline simulations.

### *a. The CCSM-driven simulations*

All CCSM-driven simulations project an increase in low-level specific humidity near the GoC and in AZ of 1 g/kg or more (fig. 6, center and right columns). The CRCM and the WRFG, two RCMs that do generate a reasonable GoC LLJ in the NCEP-driven and baseline GCM-driven runs (BUK13, their figs. 8 and 17), increase the strength of the GoC LLJ as well (fig. 6, left column). The MM5I does not have a mean GoC LLJ, and flow becomes even more northerly in the future. This difference explains why the increase in specific humidity in this simulation is not as deep, strong, and does not penetrate as far into AZ as in the CRCM and WRFG. It also supports the more uniformly negative precipitation change across AZ in the MM5I compared to the CRCM and WRFG, and the small, insignificant increase on the windward side of the Mogollon rim in the latter two. In the CRCM-ccsm and WRFG-ccsm, the changes in moisture and local flow alone imply potential for an increase in NAM system precipitation in the future in AZ and MX. However, all of these simulations start out with a strong low-bias in specific humidity (BUK13), inherited from the CCSM, and the projected increase in humidity is not enough to even compensate for the starting bias; that is, relative to historical period observations, the future simulation would still be biased dry despite the increase in humidity.

Compounding the humidity bias, and at least partly explaining the strong decrease in precipitation projected for the future regionally, is the upper-level monsoon anticyclone. The mean center of the high geopotential heights is misplaced, to start, in a position that is not favorable for good moisture flux convergence in the SWUS (e.g. fig. 7a for the 500-hPa mean high center locations for current and future). This southward displacement is associated with dry monsoon years in the SWUS (Higgins et al. 1998, Higgins and Shi 2000), though it would also usually be associated with a weaker than average anticyclone, as less precipitation (through a dry bias or in a dry year) would also lead to a low bias in the production of cloud diabatic heating of the regional atmosphere which, in turn, would likely lead to a weaker monsoon anticyclone. This is what is seen here, likely because the strength and location of the anticyclone is mostly inherited from the CCSM. Note that in these CCSM-related simulations there are often two mean, closed centers of anticyclonic circulation, one in the Southwest and one in the South-Central U.S. The entire west-to-east oriented ridge axis associated with the center of the high also exists in these simulations, but here it is connecting high centers and is also too far south. Interestingly, the CRCM-ccsm is the least incorrect here, as the location of the monsoon high is really the center of one very elongated anticyclonic circulation that stretches from central AZ into Arkansas. It is interesting that this model diverges from the others, because it is the only one of the three RCMs that includes nudging (weakly, at 500-hPa and above), which would generally make it more likely to match the large-scale pattern from the CCSM. We have no explanation for this behavior at this time.

Being too far south in most simulations, the monsoon anticyclone is producing mean flow into the SWUS that is less tropical in origin and with a greater fetch from the Pacific (i.e. in fig. 7a, the vector set in AZ from the RCMs has a greater westerly component than NCEP suggests it should). The monsoon high and mid-to-upper level heights in general are also too strong, and the heights increase in the future. Thus, the anticyclone would act to suppress convection more than normal in the baseline period and it then does so to an even greater extent in the future. Furthermore, while the westernmost center of high heights does not change its mean position, in all CCSM-related simulations there is an increase in flow that is continental in origin above 900 hPa over AZ and flow with a slightly stronger northerly component over the southern half of the GoC at 500-hPa (figs. 6 and 7a). In the CRCM and WRFG, this is associated with a well-defined future-minus-current anticyclonic flow anomaly at 500-hPa that is centered near or just northeast of the Great Salt Lake and a stronger inverted trough at 700-hPa east of the SMO (fig. 8, 500-hPa partly shown in fig. 7).

The future flow anomaly resembling a stronger inverted trough is similar to an anomaly that would precede inverted trough/tropical easterly wave (TEW) passage and often associated gulf surges[1] (Schiffer and Nesbitt 2012). However, given that there is little-to-no TEW activity in this version of the CCSM (fig. 10, McCrary et al. 2014), at least as far as TEWs originating over Africa are concerned, this is unlikely to be associated with a future change in TEW activity. The increased strength of the inverted trough to the east of the SMO in the RCMs is likely forced by an incidental change in the CCSM, and is only seen in the RCMs because it is inherited. It is not a propagating feature. In the future in the CCSM, the southward flow on the eastern side of the westernmost anticyclone center increases and the northerly flow on the western side of the easternmost anticyclone center increases. This gives the false sense of a stronger inverted trough in the anomaly field between the two anticyclonic centers (fig. 8, the cyclonic anomaly centered over far western Texas in panel a). Furthermore, in July and August, precipitation is forced, most evenings, on the east and southeast slope of the very coarse-resolution terrain that represents the Rocky Mountains and the eastern slope of the SMO related to the Gulf of Mexico (GoM) LLJ in the CCSM (not shown). This precipitation significantly increases in the future (fig. 3a), unlike the already strong monsoon-related precipitation on the western slope of the SMO in MX, and may also be increasing the strength of the existing anomalous cyclonic circulation there.

The anomalous future-minus-current anticyclonic flow in the northern Rocky Mountains, that forces an increase in continental flow in the SWUS in the future and the decrease in precipitation, is likely tied to El Niño. Castro et al. (2001) showed that anomalous ridging over



[1] Coastaly trapped wave that propagates up the GoC forced by convection associated with inverted trough/tropical easterly wave passage near the south end of the GoC (e.g. J. E. Hales 1972 and Stensrud et al. 1997).

the Northern Rockies in late June and early July, associated with the positive phase of the Pacific transition (PT) pattern, is significantly and strongly correlated with a negative/cool SST anomaly over the Niño 3 region. According to Meehl and Arblaster (2002), June-September mean negative SST anomalies in the central-to-eastern equatorial Pacific follow December-February mean positive/warm SST anomalies that are usually associated with El Niño. It follows then that a positive winter SST anomaly (El Niño) would be associated with the PT height anomaly pattern at the beginning of the NAM season seen in Castro et al. (2001). As the CCSM does project a shift to more El Niño like conditions in the future (van Oldenborgh et al. 2005), it is possible that the PT-like flow anomaly we observe is forced by this shift. However, the CCSM also has a poor representation of El Niño southern oscillation (ENSO) variability to start (too frequent and too weak, van Oldenborgh et al. 2005), and the RCMs forced by it do not well simulate ENSO-related variability of monsoon precipitation as a result (Carrillo et al. 2014), leaving confidence in these projections even lower.

In the MM5I-ccsm, the pattern of mid-level change is different (figs. 7a and 8c). It produces anomalous cyclonic flow in its 500-hPa projected difference, centered over southeast Missouri. This occurs as the inverted trough between the two anti-cyclone centers strengthens in the future, as in the CRCM- and WRFG-ccsm simulations, but to a much greater extent. The anticyclonic flow anomaly in the Northwest U.S. is not present in this simulation. The reason for the divergence of this simulation from its driver to a much greater extent than the WRFG and CRCM projections may be related to the "drift" that occurs in all MM5I simulations (and only the MM5I simulations). That is, the MM5I has a warming bias that causes it to slowly depart from its driver, any driver, rather linearly over the course of a run at all levels. In the MM5I-ccsm simulations, this leads to about a 1.14 m/year increase in 500-hPa geopotential heights over the CCSM during the baseline simulation, and a 0.86 m/year increase over the CCSM in the future, averaged over the full model domain. For additional discussion of this bias, see Bukovsky (2012).

While changes in the ingredients necessary for convection in the CCSM-driven simulations are somewhat mixed, the starting, inherited biases in these simulations that lead to little precipitation in the current period, particularly the monsoon high location and strength biases compounded by the starting humidity bias, likely lead to unrealistic and unreliable decreases in precipitation amount, frequency, and intensity over the region. Confidence in the changes in future upper-level, larger-scale flow, that would at least support a decrease in precipitation of an unknown magnitude over the SWUS, is also low, as the CCSM is one of many CMIP3 GCMs with a poor simulation of ENSO variability (Collins and the CMIP Modeling Groups 2005), and the NAM system precipitation change in the RCMs appears to be related to a questionable increase in El Niño frequency. Overall, all of these biased starting conditions act to strongly inhibit convection in the current period, to the extent that there is no monsoon precipitation signal in the annual cycle of precipitation in these models, and these biased conditions become stronger in the future, leading to an unreliably large decrease in mid-century precipitation.

*b. The CGCM-driven simulations*

Current-to-future differences in wind suggest a decrease in the strength or frequency of the inverted trough off the west coast of MX, supporting the decreases in specific humidity and precipitation. This is illustrated through figs. 7b, 9, and 11. The trough is associated with tropical easterly waves or, on occasion, tropical cyclones. It acts to transport moisture into the NAM region. Unlike the CCSM, this version of the CGCM does simulate easterly wave activity that is similar to that seen in reanalysis over Africa, at least, so TEW forcing may be included here (fig. 10, and Skinner and Diffenbaugh 2013). This future change in flow slightly decreases the specific humidity in the region during the season (fig. 9), as flow is less southerly, including that related to the GoC LLJ, for the most part. This drives decreases in precipitation in the CRCM and WRFG simulations in the SWUS and MX (fig. 3g, i). The RCM3-cgcm does not have as widespread a precipitation decrease as the other CGCM-driven simulations, but it has a small increase in humidity at the northern end of the GoC, coincident with a small increase in southerly flow there (fig. 9, center panel), that may be due to a stronger sea breeze.

The RCM3, however, is one of two RCMs that typically have a large bias in precipitation intensity (the other being ECP2), as illustrated in fig. 12. To better explain this intensity bias and its potential effect on the precipitation projections, particularly for wet and dry monsoon years, we present a Hovmoller diagram in fig. 13 for one dry and one wet year (as defined in section 3) in the historical and future simulations of the RCM3-cgcm and the CRCM-cgcm. In 1988, the wet RCM3 produces intense precipitation but events have a short duration (Fig. 13); however, the dry CRCM produces less precipitation but convection persists longer as it propagates westward over time, which is consistent with the observed propagation of precipitation in this region (e.g. Gochis et al. 2007, Lang et al. 2007, Nesbitt et al. 2008). In wet and dry years, the timing and frequency of events is similar between RCMs because they have the same parent GCM; however, in fig. 13, whether or not it is a dry or wet monsoon year, current or future, the RCM3 precipitates more heavily during any individual event than the CRCM. Therefore, the less widespread and smaller decreases in mean precipitation in the RCM3 versus the CRCM (or

WRFG) are likely the result of these differing changes in the intensity of individual events, joint with the changes in intensity and frequency seen in section 3.

The larger-scale changes in the CGCM-forced simulations do imply less precipitation, but the magnitude of the precipitation projections is still questionable, as these simulations have some of the same basic problems as the CCSM-forced simulations, and they may also be leading to a deceptively large decrease in precipitation. Unlike the CCSM-driven simulations, these runs do not simulate an overly strong monsoon high, so no deceptive response due to this error is present. However, the CGCM-driven simulations also place the mean location of the anticyclone too far south, and its position does not change much in the future, though it does strengthen. This location is not ideal for good moisture transport in the SWUS, as in section 4.a, and it is made even less ideal by a plausibly realistic change in flow in the future (decrease in the strength of the inverted trough). The CGCM-driven simulations, like the CCSM-driven simulations, also start with a large dry bias in low level specific humidity, which also causes a large low precipitation bias (BUK13). Warmer and slightly drier conditions, plus the other changes discussed above, contribute overall to an environment that is even less favorable for convection, as seen in the decrease in the frequency of precipitation of nearly all magnitudes (fig. 4), and particularly for convective initiation. For example, convective inhibition (CIN) in JA monthly mean profiles for 1981-1999 and 2051-2069[2], near Los Mochis, MX in the CRCM-cgcm projection increases from 483 J/kg to 578 J/kg, a 19% increase. In the CRCM-ncep simulation, however, mean CIN is 241 J/kg at this location, and if we simply apply the mean temperature and specific humidity changes from the CGCM-driven simulation to the CRCM-ncep profile (as in the “delta” method, but not with the climate change applied to observations), this increases to 358 J/kg. The latter is a larger

[2] An overlapping period with the NCEP-driven simulation in the baseline period and an equivalent number of years in the future.

increase in CIN, current-to-future, but the delta-method-like future value is still lower than the value from the CRCM-cgcm in the baseline period by 125 J/kg, and would be easier to overcome with any given level of forcing.

Additionally, the pattern of more anticyclonic flow west of the Baja peninsula seen in the future is correlated in observations with El Niño years and a positive North Pacific Oscillation, as shown in Castro et al. (2001). However, while the CGCM is similar to the CCSM in that it has an ENSO cycle that is too frequent and with too weak an amplitude, it instead produces a more La Niña like state in the future, like other low resolution GCMs (van Oldenborgh et al. 2005). Little confidence is assigned to this future projection of more La Niña-like conditions because of the poor ENSO simulations in the GCMs that project it (van Oldenborgh et al. 2005), and here, it is contrary to this pattern of change, implying that there is another cause for this flow anomaly. Lastly, an increase in La Niña-like years would imply more favorable conditions (e.g. enhanced GoC LLJ) and more precipitation (Castro et al. 2001), not seen here.

While it is impossible to say what the magnitude of the precipitation decrease would be if the possibly plausible larger-scale changes in flow from the CGCM-driven simulations were applied to more realistic starting conditions, it is likely that the decreases projected in these simulations are not representative of those values. Furthermore, while a decrease in precipitation would likely occur given the change in flow, the biases existing in these simulations may be leading to a greater decrease in precipitation than if the larger-scale changes were applied to non-biased starting conditions, as the convective environment is bad to start and only becomes worse in the future.

*c. The GFDL-driven simulations*

The GFDL-driven simulations' main problem, caused by the GFDL GCM which forces an incredibly excessive amount of precipitation in the NAM region from September through December, only starts to appear as a problem in August (BUK13). It is unclear what effect this bias has on projections for the core of the monsoon season. However, Carrillo et al. (2014) found that this misrepresentation of the NAM region annual cycle may cause a poor representation of the spatial variability of JA precipitation at a continental scale associated with ENSO and PDO. Relative to the CCSM- and CGCM-driven simulations, most of the GFDL-driven simulations do not have a large bias in the magnitude or location of the monsoon high (fig. 7c), except the ECP2-gfdl, in which the anticyclone is too weak. The GFDL-driven simulations do not have other, precipitation-exterminating biases in their driving fields that they inherit during JA either. However, the parent GCM is known to have very weak TEW activity (fig. 10, and Skinner and Diffenbaugh 2013), which likely contributes at least to the dry AZ precipitation biases seen in the RCMs. The other known problems in JA are largely tied to the RCMs. HRM3, for example, is the only simulation of the three that reasonably reproduces the GoC LLJ, and it projects a decrease in northward flow (not shown). During JA, however, its LLJ is too strong and too deep to start, and it maintains that problem in the future, possibly because of the large southerly flow bias it starts to inherit in August (fig. 20 in BUK13). The RCM3 does not produce a LLJ in this simulation, and does not produce a good signal for the monsoon in AZ precipitation as a result (fig. 12 in BUK13). There is little-to-no upper-level information from the ECP2-gfdl simulation available yet, but it might be assumed that it does not have the GoC LLJ as well, since the ECP2 does not produce one when driven with NCEP and this feature remains fairly consistent in quality in the other RCMs when driven with various GCMs. The HRM3 is also the only simulation of the three that does not have a high bias in the intensity of the precipitation it produces. The RCM3 and, especially, the ECP2 do (fig. 12). Moreover, it is possible that this intensity bias is contributing to the increase in precipitation seen in the ECP2-gfdl, particularly in the SWUS, where its intensity is most biased to start and it projects the greatest increase in the future (fig. 12). Unfortunately, it is not possible to further examine the ECP2-gfdl to see what is driving the relatively large precipitation increases due to the unavailability of many of its output fields. The intensity bias might also be contributing to the precipitation projections from the RCM3, as when forced with the CGCM. Without this intensity bias, it is possible that the areas where less precipitation is projected would be drier and that the increases would be weaker, given the same changes in frequency.

The decreases in future precipitation seen in the HRM3, however, are warranted given the changes in circulation and its lack of a large precipitation intensity bias. The strengthening upper-level high and small decreases in southerly flow; particularly near the GoC help explain the small, but significant decreases in precipitation in this simulation (fig. 7c). The GFDL, as well as the HADCM discussed in the next section, do not have significant future changes in ENSO, or significant problems in simulating it, as in the CGCM and CCSM (van Oldenborgh et al. 2005); therefore, they do not lose credibility from this point of view.

*d. The HADCM-driven simulations*

The HADCM-driven simulations inherit fewer biases from their parent global model than the rest (BUK13). They contain realistic NAM system precipitation during the NAM season, and although the RCMs inherit an early onset problem from the HADCM, this bias is much less fatal to the precipitation simulations than what is seen in the other GCM-driven simulations (BUK13). The HADCM also contains reasonable African TEW activity (fig. 10f). This version of the HADCM is also one of two models in the CMIP3 suite that was found to most realistically represent ENSO variability (Dominguez et al. 2010 and van Oldenborgh et al. 2005, although these analyses did not focus on the realization used for the NARCCAP simulations). However, despite having the same parent GCM and fewer initial biases, there are noticeable differences in the precipitation projections between the HADCM-forced simulations, particularly in AZ/the four-corners region and near the west coast of MX and the GoC. This is due to differences in how mid-to-upper level flow evolves in the future. The MM5I-hadcm, having no average low-level southerly flow over the GoC in the current or future simulation (no GoC LLJ), projects a decrease in northerly flow over the northern half of the GoC below about 850 hPa, likely an increase in the strength of the daily sea breeze due to an increase in the land-sea temperature contrast (fig. 14). The mean position of the monsoon anticyclone in the MM5I-hadcm is good, relative to many of the other simulations, and it does strengthen and shift slightly northeast in the future, closer the correct position in the baseline climate, as illustrated in fig. 7d. The overall change in mid-to-upper level flow in the MM5I in the future is that of an anomalous cyclone centered over the Big Bend region of Texas (partly illustrated in fig. 7d in the difference vectors to the west of the anomalous cyclone center). This is associated with a change to strong divergence on the west coast of MX at 500-hPa at the southern edge of the Sonoran desert in the future. North of the divergent point, future flow still travels anticyclonically around the high center, but south of that point, along the west coast of MX, it is northerly, on average, associated with a stronger inverted trough to the east of the SMO in the future. The switch to predominantly northeast flow near the west coast of MX in the future in the MM5I explains the decreased precipitation there. However, the reason for this peculiar larger-scale change, which is quite different from what the parent GCM does, may be related to the unrealistic "drift" in the MM5I, as discussed in section 4.a.

In the HRM3-hadcm simulation, the precipitation decrease centered on the four-corners region is likely due to an increase in mid-to-upper level northerly flow. At 500-mb, the change in the winds resembles an anomalous inverted ridge that covers the western half of the U.S., with a ridge axis running along the west coast and curving southeast through the four-corners; thus, leading to enhanced continental flow over the western half of the U.S. and stronger easterly flow over MX (not shown, but suggested in fig. 7d). This corresponds with enhanced easterlies, which force increased precipitation in eastern MX in the future. Increased moisture, and an increase in low-level southerly flow over the northern half of the GoC are not enough to counter the increased, unfavorable flow aloft, leading to the decrease in precipitation in the four-corners region.

## 5. Discussion and Conclusions

While model agreement sometimes leads to increased confidence, it can also be fairly irrelevant and potentially misleading, as in our examination. We have shown here that the NARCCAP ensemble projects decreased mean precipitation and less frequent precipitation during the NAM season in the SWUS and northwest MX with good agreement. However, after an in depth analysis of the NAM system in the 11 NARCCAP RCMs, we find that the ensemble mean precipitation projection lacks credibility. Some of the more important features analyzed, and their contribution to our conclusion on credibility are summarized in table 6. Combining this study with results from BUK13, we find that some of the most credible simulations, regarding their baseline performance and their projections, are the HADCM-driven simulations and the HRM3 simulations (including the implied overlap). These three simulations also obtain the highest numbers of positive scores in table 6. However, the HRM3-gfdl contains the unknown effect of the GFDL "extended" monsoon season and in the MM5I-hadcm, the similarly unknown effect of the MM5I "drift", leaving the HRM3-hadcm as the most credible simulation in the set. This one simulation projects small but significant decreases in mean precipitation during the core of the NAM season across the SWUS, small increases in the number of dry days regionally, and an increase in the frequency of the heaviest precipitation events with a decrease in the frequency of precipitation of lesser intensities (figs. 3 and 4 and table 3).

The WRFG-cgcm and CRCM-cgcm simulations could be considered "runners-up" behind the previously described simulations, but they have biases inherited from the CGCM that cause their projections to be much more questionable. Given that the WRFG and CRCM perform well when forced with NCEP for the NAM system, it would be ideal to complete simulations where they are forced with a less biased set of GCMs (e.g. HADCM), but this is outside the scope of this study and the planned set of NARCCAP simulations. Here the value added by the WRFG and CRCM to their coarse resolution drivers through the addition of finer-scale forcing and appropriate mesoscale features (e.g. local orography like the Mogollon Rim and GoC, and RCM-developed circulations like the GoC LLJ) is eclipsed by the problems caused by the biased boundary conditions from the CGCM (and the CCSM).

The poorest simulation is the MM5I-ccsm (table 6). Note that this simulation includes the large-scale disadvantages of the CCSM (which leads to the lowest average positive responses in all of the RCMs it forces in table 6) along with the relatively poor performance of the MM5I regarding sub-regional scale phenomenon (e.g., the GoC LLJ). Certainly we discourage the use of the MM5I-ccsm results in this region for, say, an impacts analysis, nor should it be included in an ensemble of NARCCAP results for this region.

It is important to note that while our more credible simulations generally produced a smaller signal for a decrease in mean NAM precipitation amount by mid-century, this would not necessarily preclude drying in the region, as temperatures are also projected to rise, and soil moisture evaporation would increase. Exploring this effect is outside the capacity of this manuscript, however.

The effect of the GCM-bias on our RCM simulations encapsulates the well known "garbage in-garbage out" effect (e.g. Rummukainen 2010), and it governs four of the six specifically named features in table 6. This can be used to argue that a GCM can not be too skillful for further downscaling (contrary to a statement in Shindell et al. 2014 that GCMs "should not be too skillful...or there will be little opportunity for added value") and that the careful selection of GCMs for downscaling is warranted. However, picking a "good" GCM for downscaling is clearly not a straightforward task, particularly for large, diverse regions, like the NARCCAP North American domain.

It has been noted in numerous publications that it is difficult to evaluate GCM and RCM simulations in order to either eliminate ensemble members (of too poor quality) or differentially weight them for the sake of coming up with more robust estimates of future climate on regional scales (e.g., Gleckler et al. 2008, Knutti et al. 2010, Bukovsky et al. 2014). This problem persists, and we would likely have a difficult time determining if some of these NARCCAP simulations should be used for any purpose over this region aside from general research on model results. Yet we do believe we have made headway in applying regional, process-based methods to evaluate the quality of future projections (Barsugli et al. 2013). We have at least determined both the best and the worst simulations and can make recommendations about their use. Essentially, for some purposes, we might recommend using only the HRM3-hadcm. However, the NARCCAP simulations do not fully represent the uncertainty space characterized by a full suite of GCMs (e.g., CMIP3 or CMIP5) or multiple emissions/concentration scenarios. The range of the equilibrium climate sensitivity covered by the four NARCCAP driving GCMs is 2.7 – 3.4 ºC, whereas the full CMIP3 suite covers 2.1 – 4.4 ºC. We note this because, although NARCCAP was constructed for use in impacts and adaptation studies (Mearns et al. 2009), it is also known that it does not completely cover the known and quantifiable uncertainty space. Hence, recommending the use of a single NARCCAP simulation may not be justified in this case for this region.

Finally, we hope to take what we have learned in this work with NARCCAP and some of the CMIP3 GCMs and expand on it in the near future with the CMIP5 and CORDEX ensembles.

*ACKNOWLEDGEMENTS*

We wish to thank NARCCAP for providing the data used in this paper. NARCCAP is funded by the National Science Foundation, the U.S. Department of Energy, the National Oceanic and Atmospheric Administration (NOAA), and the U.S. Environmental Protection Agency Office of Research and Development. We would also like to thank the entire NARCCAP modeling team for useful discussions regarding this work. The authors also acknowledge the support of the NOAA Climate Program Office Modeling, Analysis, Predictions and Projections (MAPP) Program. Work was supported under grant # NA11AOR4310111

## REFERENCES


Barsugli, J. J., G. Guentchev, R. M. Horton, A. Wood, L. O. Mearns, X. Z. Liang, J. A. Winkler, K. Dixon, K. Hayhoe, R. B. Rood, L. Goddard, A. Ray, L. Buja, and C. Ammann, 2013: The practitioner's dilemma: How to assess the credibility of downscaled climate projections. Eos, Trans. Amer. Geophys. Union, 94, 424–425, doi:10.1002/2013EO460005.

Bukovsky, M. S., 2012: Temperature trends in the NARCCAP regional climate models. J. Climate, 25, 3985–3991.

Bukovsky, M. S., D. J. Gochis, and L. O. Mearns, 2013: Towards assessing NARCCAP regional climate model credibility for the North American monsoon: Current climate simulations. J. Climate, 26, 8802–8826, doi:10.1175/JCLI-D-11-00588.1.

Bukovsky, M. S. and D. J. Karoly, 2011: A regional modeling study of climate change impacts on warm-season precipitation in the central United States. J. Climate, 24, 1985–2002, doi:10.1175/2010JCLI3447.1.

Bukovsky, M. S., J. Thompson, and L. O. Mearns, 2014: Does weighting make a difference? The effect of weighting on the NARCCAP ensemble mean. To be submitted to Climate Research November 2014.

Carrillo, C. M., C. L. Castro, G. Garfin, H. Chang, and M. S. Bukovsky, 2014: Evaluation of the ENSO and PDV natural climate variability on the North American monsoon region using a set of CMIP3 dynamically downscaled products from NARCCAP. To be submitted to Int. J. Climatol.

Castro, C. L., H. Chang, F. Dominguez, C. Carrillo, J. K. Schemm, and H. M. H. Juang, 2012: Can a regional climate model improve the ability to forecast the North American monsoon? J. Climate, 25, 8212–8236, doi:10.1175/JCLI-D-11-00441.1.

Castro, C. L., T. B. McKee, and S. R. A. Pielke, 2001: The relationship of the North American Monsoon to tropical and North Pacific sea surface temperatures as revealed by observations. J. Climate, 14, 4450–4473.

Castro, C. L., S. R. A. Pielke, and J. O. Adegoke, 2007a: Investigation of the summer climate of the contiguous United States and Mexico using the regional atmospheric modeling system (RAMS). Part I: model climatology (1950-2002). J. Climate, 20, 3844–3865.

Castro, C. L., S. R. A. Pielke, J. O. Adegoke, S. D. Schubert, and P. J. Pegion, 2007b: Investigation of the summer climate of the contiguous United States and Mexico using the regional atmospheric modeling system (RAMS). Part II: model climate variability. J. Climate, 20, 3866–3887.

Caya, D. and R. Laprise, 1999: A semi-implicit semi-Lagrangian regional climate model: The Canadian RCM. Mon. Wea. Rev., 127, 341–362, doi:10.1175/1520-0493(1999)127<0341:ASISLR>2.0.CO;2.

Christensen, J. H., B. Hewitson, A. Busuioc, A. Chen, X. Gao, I. M. Held, R. Jones, R. K. Kolli, W. T. Kwon, R. Laprise, V. M. Rueda, L. Mearns, C. G. Menéndez, J. Räisänen, A. Rink, A. Sarr, and P. Whetton, 2007: Climate Change 2007: The Physical Science Basis. Contribution of Working Group I to the Fourth Assessment Report of the Intergovernmental Panel on Climate Change, Cambridge University Press, Cambridge, United Kingdom and New York, NY, USA, Chap. Regional Climate Projections, 94.

Collier, J. C. and G. J. Zhang, 2007: Effects of increased horizontal resolution on simulation of the North American monsoon in the NCAR CAM3: An evaluation based on surface, satellite, and reanalysis data. J. Climate, 20, 1843–1862, doi:10.1175/JCLI4099.1.

Collins, M. and the CMIP Modeling Groups, 2005: El Niño- or La Niña-like climate change? Clim. Dyn., 24, 89–104.

Collins, W. D., C. M. Bitz, M. L. Blackmon, G. B. Bonan, C. S. Bretherton, J. A. Carton, P. Chang, S. C. Doney, J. J. Hack, T. B. Henderson, J. T. Kiehl, W. G. Large, D. S. McKenna, B. D. Santer, and R. D. Smith, 2006: The Community Climate System Model: CCSM3. J. Climate, 19, 2122–2143, doi:10.1175/JCLI3761.1.

Cook, B. I. and R. Seager, 2013: The response of the North American monsoon to increased greenhouse gas forcing. J. Geophys. Res. Atmos., 118, 1690–1699, doi:10.1002/jgrd.50111.

Dee, D. P., S. M. Uppala, A. J. Simmons, P. Berrisford, P. Poli, S. Kobayashi, U. Andrae, M. A. Balmaseda, G. Balsamo, P. Bauer, P. Bechtold, A. C. M. Beljaars, L. van de Berg, J. Bidlot, N. Bormann, C. Delsol, R. Dragani, M. Fuentes, A. J. Geer, L. Haimberger, S. B. Healy, H. Hersbach, E. V. Hólm, L. Isaksen, P. Kållberg, M. Köhler, M. Matricardi, A. P. McNally, B. M. Monge-Sanz, J. J. Morcrette, B. K. Park, C. Peubey, P. de Rosnay, C. Tavolato, J. N. Thépaut, and F. Vitart, 2011: The ERA-Interim reanalysis: configuration and performance of the data assimilation system. Quart. J. Roy. Meteor. Soc., 137, 553–597.

Dominguez, F., J. Cañon, and J. Valdez, 2010: IPCC-AR4 climate simulations for the southwestern US: the importance of future ENSO projections. Climatic Change, 99, 499–514.

Efron, B. and R. Tibshirani, 1993: An introduction to the bootstrap. Chapman and Hall/CRC, 450 pp.

Flato, G. M., G. J. Boer, W. G. Lee, N. A. McFarlane, D. Ramsden, M. C. Reader, and A. J. Weaver, 2000: The Canadian Centre for Climate Modeling and Analysis global coupled model and its climate. Clim. Dynam., 16, 451–467, doi:10.1007/s003820050339.

Gao, Y., L. R. Leung, E. P. Salathé, F. Dominguez, B. Nijssen, and D. P. Lettenmaier, 2012: Moisture flux convergence in regional and global climate models: Implications for droughts in the southwestern United States under climate change. Geophys. Res. Lett., 39, L09 711.

Geil, K. L., Y. L. Serra, and X. Zeng, 2013: Assessment of CMIP5 model simulations of the North American Monsoon system. J. Climate, 26, 8787–8801.

GFDL GAMDT, 2004: The new GFDL global atmosphere and land model AM2-LM2: Evaluation with prescribed SST simulations. J. Climate, 17, 4641–4673, doi:10.1175/JCLI-3223.1.

Giorgi, F., M. R. Marinucci, and G. T. Bates, 1993a: Development of a second-generation Regional Climate Model (RegCM2). Part I: Boundary-layer and radiative transfer processes. Mon. Wea. Rev., 121, 2794–2813, doi:10.1175/1520-0493(1993)121<2794:DOASGR>2.0.CO;2.

Giorgi, F., M. R. Marinucci, G. de Canio, and G. T. Bates, 1993b: Development of a second-generation Regional Climate Model (RegCM2). Part II: Convective processes and assimilation of lateral boundary conditions. Mon. Wea. Rev., 121, 2814–2832, doi:10.1175/1520-0493(1993)121<2814:DOASGR>2.0.CO;2.

Gleckler, P. J., K. E. Taylor, and C. Doutriaux, 2008: Performance metrics for climate models. J. Geophys. Res., D06104, doi:10.1029/2007JD008972.

Gochis, D. J., C. J. Watts, J. Garatuza-Payan, and J. C. Rodriguez, 2007: Spatial and temporal patterns of precipitation intensity as observed by the NAME Event Rain Gauge Network from 2002-2004. J. Climate, 20, 1734–1750.

Gordon, C., C. Cooper, C. A. Senior, H. Banks, J. M. Gregory, T. C. Johns, J. F. B. Mitchell, and R. A. Wood, 2000: The simulation of SST, sea ice extents and ocean heat transports in a version of the Hadley Centre coupled model without flux adjustments. Clim. Dynam., 16, 147–168, doi:10.1007/s003820050010.

Grell, G. A., J. Dudhia, and D. R. Stauffer, 1993: A description of the fifth-generation Penn State/ NCAR Mesoscale Model (MM5). NCAR Tech. Note NCAR/TN-398+1A.

Gutzler, D. S., L. N. Long, J. Schemm, S. B. Roy, M. Bosilovich, J. C. Collier, M. Kanamitsu, P. Kelly, D. Lawrence, M. I. Lee, R. L. Sánchez, B. Mapes, K. Mo, A. Nunes, E. A. Ritchie, J. Roads, S. Schubert, H. Wei, and G. J. Zhang, 2009: Simulations of the 2004 North American monsoon: NAMAP2. J. Climate, 22, 6716–6740, doi:10.1175/2009JCLI3138.1.

Higgins, R. W., K. C. Mo, and Y. Yao, 1998: Interannual variability of the U.S. summer precipitation regime with emphasis on the Southwestern monsoon. J. Climate, 11, 2582–2606.

Higgins, R. W. and W. Shi, 2000: Dominant factors responsible for interannual variability of the summer monsoon in the southwestern United States. J. Climate, 13, 759–775.

Hoerling, M. and J. Eischeid, 2007: Past peak water in the Southwest. Southwest Hydrology, 18, 18–19.

IPCC, 2000: Special Report on Emissions Scenarios. Cambridge University Press, Cambridge, UK, 432 pp.

J. E. Hales, J., 1972: Surges of maritime tropical air northward over the Gulf of California. Mon. Wea. Rev., 100, 298–306.

Jones, R. G., D. C. Hassell, D. Hudson, S. S. Wilson, G. J. Jenkins, and J. F. B. Mitchell, 2003: Workbook on generating high-resolution climate change scenarios using PRECIS. UNDP.

Juang, H. M., S. Y. Hong, and M. Kanamitsu, 1997: The NCEP regional spectral model. An update. Bull. Amer. Meteor. Soc., 78, 2125–2143, doi:10.1175/1520477(1997)078<2125:TNRSMA>2.0.CO;2.

Kanamitsu, M., W. Ebisuzaki, J. Woollen, S. K. Yang, J. J. Hnilo, M. Fiorino, and G. L. Potter, 2002: NCEP-DOE AMIP-II Reanalysis (R-2). Bull. Amer. Meteor. Soc., 83, 1631–1643.

Knutti, R., G. Abramowitz, M. Collins, V. Eyring, P. J. Gleckler, and L. Mearns, 2010: Meeting Report of the Intergovernmental Panel on Climate Change Expert Meeting on Assessing and Combining Multi Model Climate Projections, IPCC Working Group I Technical Support Unite, University of Bern, Bern Switzerland, Chap. Good Practice Guidance Paper on Assessing and Combining Multi Model Climate Projections.

Lang, T. J., D. A. Ahijevych, S. W. Nesbitt, R. E. Carbone, S. A. Rutledge, and R. Cifelli, 2007: Radar-observed characteristics of precipitating systems during NAME 2004. J. Climate, 20, 1713–1733.

Lee, M. I., S. D. Schubert, M. J. Suarez, I. M. Held, A. Kumar, T. L. Bell, J. K. E. Schemm, N. C. Lau, J. J. Ploshay, H. K. Kim, and S. H. Yoo, 2007: Sensitivity to horizontal resolution in the AGCM simulations of warm season diurnal cycle of precipitation over the United States and northern Mexico. J. Climate, 20, 1862–1881, doi:10.1175/JCLI4090.1.

Lin, J. L., B. E. Mapes, K. M. Weickmann, G. N. Kiladis, S. D. Schubert, M. J. Suarez, J. T. Bacmeister, and M. I. Lee, 2008: North American monsoon and convectively coupled equatorial waves simulated by IPCC AR4 coupled GCMs. J. Climate, 21, 2919–2937.

McCrary, R. R., D. A. Randall, and C. Stan, 2014: Simulations of the West African monsoon with a super-parameterized climate model. Part 2: African easterly waves. J. Climate, Submitted.

McKee, T. B., N. J. Doeskin, and J. Kleist, 1993: The relationship of drought frequency and duration to time scales. Proc. 8th Conf. on Applied Climatology, Boston, MA, Amer. Meteor. Soc., 179–184.

Mearns, L., R. Arritt, S. Biner, M. S. Bukovsky, S. McGinnis, S. Sain, D. Caya, J. J. Correia, D. Flory, W. Gutowski, E. S. Takle, R. Jones, L. R. Leung, W. Moufouma-Okia, L. McDaniel, A. Nunes, Y. Qian, J. Roads, L. Sloan, and M. Snyder, 2012: The North American Regional Climate Change Assessment Program: Overview of phase I results. Bull. Amer. Meteor. Soc., 93, 1337–1362, doi:10.1175/BAMS-D-11-00223.1.

Mearns, L. O., W. J. Gutowski, R. Jones, L. Y. Leung, S. McGinnis, A. M. B. Nunes, and Y. Qian, 2009: A regional climate change assessment program for North America. Eos, Trans. Amer. Geophys. Union, 90, 311, doi:10.1029/2009EO360002.

Mearns, L. O., S. Sain, L. R. Leung, M. S. Bukovsky, S. McGinnis, S. Biner, D. Caya, R. W. Arritt, W. Gutowski, E. S. Takle, M. Snyder, R. G. Jones, A. M. B. Nunes, S. Tucker, D. Herzmann, L. McDaniel, and L. Sloan, 2013: Climate change projections of the North American Regional Climate Change Assessment Program (NARCCAP). Climatic Change, doi:10.1007/s10584-013-0831-3.

Meehl, G. A. and J. M. Arblaster, 2002: The tropospheric biennial oscillation and Asian-Australian monsoon rainfall. J. Climate, 15, 722–744.

Mesinger, F., G. DiMego, E. Kalnay, K. Mitchell, P. C. Shafran, W. Ebisuzaki, D. Jovic, J. Woollen, E. Rogers, E. H. Berbery, M. B. Ek, Y. Fan, R. Grumbine, W. Higgins, H. Li, Y. Lin, G. Manikin, D. Parrish, and W. Shi, 2006: North American regional reanalysis. Bull. Amer. Meteor. Soc., 87, 343–360.

Milly, P. C. D., K. A. Dunne, and A. V. Vecchia, 2005: Global pattern of trends in streamflow and water availability in a changing climate. Nature, 438, 347–350, doi:10.1038/nature04312.

Mitchell, D. L., D. Ivanova, R. Rabin, T. J. Brown, and K. Redmon, 2002: Gulf of California sea surface temperatures and the North American monsoon: Mechanistic implications from observations. J. Climate, 15, 2261–2281, doi:10.1175/1520-0442(2002)015<2261:GOCSST>2.0.CO;2.

Nesbitt, S. W., D. J. Gochis, and T. J. Lang, 2008: The diurnal cycle of clouds and precipitation along the Sierra Madre Occidental observed during NAME-2004: Implications for warm season precipitation estimation in complex terrain. J. Hydrometeorology, 9, 728–743.

Pal, J. S. and Coauthors, 2007: Regional climate modeling for the developing world: The ICTP RegCM3 and RegCNET. Bull. Amer. Meteor. Soc., 88, 1395–1409, doi:10.1175/BAMS-88-9-1395.

Pope, V. D., M. L. Gallani, P. R. Rowntree, and R. A. Stratton, 2000: The impact of new physical parameterizations in the Hadley Centre climate model: HadAM3. Clim. Dynam., 16, 123–146, doi:10.1007/s003820050009.

Rummukainen, M., 2010: State-of-the-art with regional climate models. Clim. Change, 1, 82–96.

Schiffer, N. J. and S. W. Nesbitt, 2012: Flow, moisture, and thermodynamic variability associated with Gulf of California surges within the North American monsoon. J. Climate, 25, 4220–4241.

Seager, R., M. Ting, I. Held, Y. Kushnir, J. Lu, G. Vecchi, H. P. Huang, N. Harnick, A. Leetmaa, N. C. Lau, C. Li, J. Velez, and N. Naik, 2007: Model projections of an imminent transistion to a more arid climate in southwestern North America. Science, 316, 1181–1184, doi:10.1126/science.1139601.

Seth, A., S. A. Rauscher, M. Biasutti, A. Giannini, S. J. Camargo, and M. Rojas, 2013: CMIP5 projected changes in the annual cycle of precipitation in monsoon regions. J. Climate, 26, 7328–7351, doi:10.1175/JCLI-D-12-00726.1.

Seth, A., S. A. Rauscher, M. Rojas, A. Giannini, and S. J. Camargo, 2011: Enhanced spring convective barrier for monsoons in a warmer world? Clim. Change, 104, 403–414, doi:10.1007/s10584-010-9973-8.

Shindell, D., P. Racherla, and G. Milly, 2014: Reply to comment by Laprise on "The added value to global model projections of climate change by dynamical downscaling: A case study over the continental U.S. using the GISS-ModelE2 and WRF models". J. Geophys. Res. Atmos., 119, 3882–3885, doi:doi:10.1002/2013JD020732.

Skamarock, W. C., J. B. Klemp, J. Dudhia, D. O. Gill, D. M. Barker, W. Wang, and J. G. Powers, 2005: A description of the Advanced Research WRF version 2. NCAR Tech. Note NCAR/TN-468+STR.

Skinner, C. B. and N. S. Diffenbaugh, 2013: The contribution of African easterly waves to monsoon precipitation in the CMIP3 ensemble. J. Geophys. Res. Atmos., 118, 3590–3609, doi:10.1002/jgrd.50363.

Solomon, S., D. Qin, M. Manning, R. B. Alley, T. Berntsen, N. L. Bindoff, Z. Chen, A. Chidthaisong, J. M. Gregory, G. C. Hegerl, M. Heimann, B. Hewitson, B. J. Hoskins, F. Joos, J. Jouzel, V. Kattsov, U. Lohmann, T. Matsuno, M. Molina, N. Nicholls, J. Overpeck, G. Raga, V. Ramaswamy, J. Ren, M. Rusticucci, R. Somerville, T. F. Stocker, P. Whetton, R. A. Wood, and D. Wratt, 2007: Climate Change 2007: The Physical Science Basis. Contribution of Working Group I to the Fourth Assessment Report of the Intergovernmental Panel on Climate Change, Cambridge University Press, Cambridge, United Kingdom and New York, NY, USA, Chap. Technical Summary.

Stensrud, D. J., R. L. Gall, and M. K. Nordquist, 1997: Surges over the Gulf of California during the Mexican monsoon. Mon. Wea. Rev., 125, 417–437.

Stocker, T. F., D. Qin, G. K. Plattner, L. V. Alexander, S. K. Allen, N. L. Bindoff, F. M. Bréon, J. A. Church, U. Cubasch, S. Emori, P. Forster, P. Friedlingstein, N. Gillett, J. M. Gregory, D. L. Hartmann, E. Jansen, B. Kirtman, R. Knutti, K. K. Kumar, P. Lemke, J. Marotzke, V. Masson-Delmotte, G. A. Meehl, I. I. Mokhov, S. Piao, V. Ramaswamy, D. Randall, M. Rhein, M. Rojas, C. Sabine, D. Shindell, L. D. Talley, D. G. Vaughan, and S. P. Xie, 2013: Climate Change 2013: The Physical Science Basis. Contribution of Working Group I to the Fifth Assessment Report of the Intergovernmental Panel on Climate Change, Cambridge University Press, Cambridge, United Kingdom and New York, NY, USA, Chap. Technical Summary.

Tebaldi, C., J. M. Arblaster, and R. Knutti, 2011: Mapping model agreement on future climate projections. Geophys. Res. Lett., 38, L23 701, doi:10.1029/2011GL049863.

Torres-Alavez, A., T. Cavazos, and C. Turrent, 2014: Land-sea thermal contrast and intensity of the North American monsoon under climate change conditions. J. Climate, 27, 4566–4580.

van Oldenborgh, G. J., S. Y. Philip, and M. Collins, 2005: El Niño in a changing climate: a multi-model study. Ocean Sci., 1, 81–95.

von Storch, H. and F. W. Zwiers, 1999: Statistical Analysis in Climate Research. Cambridge University Press, Cambridge, UK, 484 pp.

TABLE 1. RCMs and GCMs used in NARCCAP, their identifying acronyms (RCM acronyms are as used in the NARCCAP model archive), and relevant references. For the GCMs, horizontal resolution and CMIP3 archive ensemble member number are also listed.

| **Acronyms** | **RCMs** |
| --- | --- |
| CRCM | Canadian RCM; Caya and Laprise (1999) |
| ECP2 | Experimental Climate Prediction Center's version of the Regional Spectral Model; Juang et al. (1997) |
| HRM3 | Third-generation Hadley Centre RCM; Jones et al. (2003) |
| MM5I | Fifth-generation Pennsylvania State University – National Center for Atmospheric Research (NCAR) Mesoscale Model; Grell et al. (1993) |
| RCM3 | International Centre for Theoretical Physics RCM version 3; Giorgi et al. (1993a), Giorgi et al. (1993b), Pal and Coauthors (2007) |
| WRFG | Weather Research and Forecasting model; Skamarock et al. (2005) |
| | **GCMs** |
| CCSM | NCAR CCSM version 3.0, T85 (1.4 × 1.4°), run 5; Collins et al. (2006) |
| CGCM | Canadian Global Climate Model version 3, T47 (1.9 × 1.9°), run 4; Flato et al. (2000) |
| GFDL | GFDL climate model version 2.0, 2.0 × 2.5°, run 2; GFDL GAMDT (2004) |
| HADCM | Hadley Centre Climate Model version 3, 2.5 × 3.75°, this run is not part of the CMIP3 archive; Gordon et al. (2000), Pope et al. (2000) |

TABLE 2. NARCCAP RCM+GCM simulations. All planned combinations are marked. Those used here are marked with X, those not yet available with *.

| | CCSM | CGCM | GFDL | HADCM |
|---|---|---|---|---|
| CRCM | X | X | | |
| ECP2 | | | X | * |
| HRM3 | | | X | X |
| MM5I | X | | | X |
| RCM3 | | X | X | |
| WRFG | X | X | | |

TABLE 3. JA future-minus-current difference in: average precipitation (Avg, given in % and mm/day), precipitation intensity (Int, %), and the number of dry days (DD, %) for the entire analysis region over land only and the AZ and MX subregions (as shown in fig. 1). The ensemble averages for each statistic are given in the last five rows for the full ensemble with all 11 options, and then for sub-ensembles of models grouped by forcing GCM. In the “Average” row only, bold values indicate significance, and italicized values indicate strong bias in the baseline value (see section 2 for details). The four underlined values in the last 3 rows are explained in the text.

| | NAM Region | | | | AZ | | | | Mexico | | | |
|---|---|---|---|---|---|---|---|---|---|---|---|---|
| | Avg % | Avg mm/d | Int % | DD % | Avg % | Avg mm/d | Int % | DD % | Avg % | Avg mm/d | Int % | DD % |
| CRCM-ccsm | -21.30 | -0.18 | -4.04 | 7.38 | -16.73 | -0.10 | -2.53 | 4.85 | -18.45 | -0.37 | -0.58 | 15.16 |
| MM5I-ccsm | -37.13 | -0.16 | -11.95 | 4.60 | -43.53 | -0.06 | -10.40 | 2.18 | -37.86 | -0.45 | -17.35 | 10.00 |
| WRFG-ccsm | -26.16 | -0.11 | -11.07 | 3.45 | -3.91 | -0.01 | 7.21 | 0.75 | -37.67 | -0.28 | -14.77 | 8.29 |
| CRCM-cgcm | -25.29 | -0.34 | -9.96 | 10.46 | -37.63 | -0.24 | -19.01 | 7.26 | -38.31 | -1.10 | -20.77 | 23.77 |
| RCM3-cgcm | -30.59 | -0.19 | -6.66 | 3.97 | -32.56 | -0.04 | 7.31 | 0.96 | -62.82 | -0.45 | -23.38 | 8.13 |
| WRFG-cgcm | -21.79 | -0.14 | -8.73 | 3.81 | -40.49 | -0.09 | -5.08 | 3.43 | -53.07 | -0.44 | -30.48 | 9.56 |
| ECP2-gfdl | 5.52 | 0.07 | 0.39 | -1.08 | 33.44 | 0.20 | 13.15 | -1.92 | 8.52 | 0.24 | 1.89 | -2.79 |
| HRM3-gfdl | -11.79 | -0.24 | -5.98 | 6.29 | -17.59 | -0.24 | -6.32 | 9.34 | -3.11 | -0.15 | 4.62 | 30.29 |
| RCM3-gfdl | -6.57 | -0.11 | 3.76 | 3.22 | 3.46 | 0.02 | 4.75 | 0.15 | -10.39 | -0.57 | -4.46 | 4.35 |
| HRM3-hadcm | -3.35 | -0.06 | 2.84 | 5.47 | -25.17 | -0.23 | -14.09 | 8.66 | 3.97 | 0.12 | 7.11 | 5.45 |
| MM5I-hadcm | 3.24 | 0.08 | 6.63 | 1.89 | -0.32 | -0.01 | 2.17 | 0.97 | -21.46 | -1.38 | -1.46 | 26.99 |
| Average | **-15.93** | **-0.13** | -4.07 | ***4.50*** | *-16.46* | *-0.08* | -2.08 | ***3.33*** | **-24.60** | **-0.48** | -9.06 | ***12.66*** |
| CCSM-driven | -28.20 | -0.15 | -9.02 | 5.14 | -21.39 | -0.05 | -1.91 | 2.59 | -31.33 | -0.37 | -10.90 | 11.15 |
| CGCM-driven | -25.89 | -0.22 | -8.45 | 6.08 | -36.89 | -0.12 | -5.59 | 3.88 | -51.40 | -0.66 | -24.88 | 13.82 |
| GFDL-driven | -4.28 | -0.09 | -0.61 | 2.81 | 6.44 | 0.00 | 3.86 | 2.52 | -1.66 | -0.16 | 0.68 | 10.62 |
| HADCM-driven | -0.05 | 0.01 | 4.73 | 3.68 | -12.75 | -0.12 | -5.96 | 4.82 | -8.74 | -0.63 | 2.83 | 16.22 |

TABLE 4. JA percent change in the amplitude and frequency of daily precipitation at the given quantiles for wet years only between the baseline and the future. The upper table shows the change in amplitude, where each column represents a specific quantile threshold. The lower table shows the frequency change in daily precipitation defined for the quantiles in the upper table. The ensemble average for each quantile is given in the last five rows for the full 11-simulation ensemble and then for sub-ensembles grouped by forcing GCM.

AMPLITUDE (%)

| Quantiles | 0.25 | 0.5 | 0.75 | 0.95 | 0.99 |
|---|---|---|---|---|---|
| CRCM_ccsm | -19.6 | -22.9 | -16.4 | 12.9 | 27.0 |
| MM5I_ccsm | -57.8 | -60.6 | -52.0 | -13.7 | -11.1 |
| WRFG_ccsm | -63.6 | -41.3 | -30.7 | -21.7 | -9.4 |
| CRCM_cgcm | -35.1 | -28.7 | -28.2 | -12.7 | -10.4 |
| RCM3_cgcm | -60.2 | -54.4 | -37.6 | -17.7 | 24.9 |
| WRFG_cgcm | -53.4 | -46.2 | -35.5 | -23.0 | -34.3 |
| ECP2_gfdl | 51.6 | 44.2 | 24.5 | 13.3 | 26.6 |
| HRM3_gfdl | -18.3 | -17.9 | -9.4 | -7.9 | -7.8 |
| RCM3_gfdl | -7.9 | 4.5 | -3.9 | -9.7 | 8.8 |
| HRM3_hadcm | -5.5 | -6.9 | 9.9 | 20.7 | 40.1 |
| MM5I_hadcm | -5.7 | 7.5 | 12.9 | 10.3 | 7.9 |
| AVERAGE | -25.1 | -20.2 | -15.1 | -4.5 | 5.7 |
| CCSM-driven | -47.0 | -41.6 | -33.0 | -7.5 | 2.2 |
| CGCM-driven | -49.6 | -43.1 | -33.8 | -17.8 | -6.6 |
| GFDL-driven | 8.5 | 10.3 | 3.7 | -1.4 | 9.2 |
| HADCM-driven | -5.6 | 0.3 | 11.4 | 15.5 | 24.0 |

FREQUENCY (%)

| Quantiles | 0.25 | 0.5 | 0.75 | 0.95 | 0.99 |
|---|---|---|---|---|---|
| CRCM_ccsm | 15.4 | -52.3 | -48.7 | 25.0 | 300.0 |
| MM5I_ccsm | 117.5 | -47.6 | -61.3 | -16.7 | 0.0 |
| WRFG_ccsm | 3.8 | -66.5 | -61.5 | -81.3 | -33.3 |
| CRCM_cgcm | 117.9 | -50.6 | -53.8 | -43.8 | -66.7 |
| RCM3_cgcm | 66.7 | -55.1 | -57.7 | -43.8 | 100.0 |
| WRFG_cgcm | 116.7 | -49.0 | -51.3 | -56.3 | -100.0 |
| ECP2_gfdl | -30.6 | 79.8 | 109.7 | 50.0 | 450.0 |
| HRM3_gfdl | 48.7 | -20.6 | -19.2 | -68.8 | -33.3 |
| RCM3_gfdl | 87.2 | 78.5 | 48.9 | 22.2 | 150.0 |
| HRM3_hadcm | -10.7 | -30.0 | -6.7 | 106.7 | 300.0 |
| MM5I_hadcm | 6.7 | 11.3 | 33.3 | 46.7 | 66.7 |
| AVERAGE | 49.0 | -18.4 | -15.3 | -5.4 | 103.0 |
| CCSM-driven | 45.6 | -55.4 | -57.2 | -24.3 | 88.9 |
| CGCM-driven | 100.4 | -51.6 | -54.3 | -47.9 | -22.2 |
| GFDL-driven | 35.1 | 45.9 | 46.5 | 1.2 | 188.9 |
| HADCM-driven | -2.0 | -9.3 | 13.3 | 76.7 | 183.3 |

TABLE 5. As in table 4, but for dry years only.

AMPLITUDE (%)

| Quantiles | 0.25 | 0.5 | 0.75 | 0.95 | 0.99 |
|---|---|---|---|---|---|
| CRCM_ccsm | -38.0 | -29.9 | -25.0 | -16.2 | -16.1 |
| MM5I_ccsm | -54.2 | -45.2 | -40.0 | -32.2 | -46.7 |
| WRFG_ccsm | -56.1 | -58.5 | -53.8 | -43.2 | -10.7 |
| CRCM_cgcm | -31.1 | -29.9 | -26.4 | -25.7 | -18.1 |
| RCM3_cgcm | -48.8 | -39.9 | -42.7 | -35.2 | -37.6 |
| WRFG_cgcm | -41.0 | -17.8 | 0.7 | -14.8 | 14.8 |
| ECP2_gfdl | 5.1 | -7.7 | -0.3 | 5.0 | -11.2 |
| HRM3_gfdl | -10.9 | -13.0 | -7.5 | -2.1 | -7.2 |
| RCM3_gfdl | -47.4 | -27.2 | -9.3 | -18.3 | -19.0 |
| HRM3_hadcm | -17.8 | -18.8 | -11.6 | -3.6 | 30.9 |
| MM5I_hadcm | -1.7 | 1.7 | 2.9 | -4.4 | 20.7 |
| AVERAGE | -31.1 | -26.0 | -19.4 | -17.3 | -9.1 |
| CCSM-driven | -49.4 | -44.5 | -39.6 | -30.5 | -24.5 |
| CGCM-driven | -40.3 | -29.2 | -22.8 | -25.3 | -13.6 |
| GFDL-driven | -17.7 | -15.9 | -5.7 | -5.1 | -12.5 |
| HADCM-driven | -9.7 | -8.6 | -4.3 | -4.0 | 25.8 |

FREQUENCY (%)

| Quantiles | 0.25 | 0.5 | 0.75 | 0.95 | 0.99 |
|---|---|---|---|---|---|
| CRCM_ccsm | 102.6 | -48.4 | -57.7 | -43.8 | -66.7 |
| MM5I_ccsm | 63.5 | -32.3 | -39.7 | -100.0 | -100.0 |
| WRFG_ccsm | 45.2 | -64.3 | -69.4 | -83.3 | -33.3 |
| CRCM_cgcm | 93.6 | -46.5 | -65.4 | -75.0 | -100.0 |
| RCM3_cgcm | 25.3 | -49.7 | -66.7 | -81.3 | -66.7 |
| WRFG_cgcm | 21.8 | -24.5 | -20.0 | -43.8 | 0.0 |
| ECP2_gfdl | -61.5 | -62.6 | -60.3 | -56.3 | -75.0 |
| HRM3_gfdl | 12.8 | -32.9 | -32.1 | -25.0 | -100.0 |
| RCM3_gfdl | 84.6 | -17.3 | -30.8 | -50.0 | -100.0 |
| HRM3_hadcm | 2.7 | -36.7 | -44.0 | -26.7 | 66.7 |
| MM5I_hadcm | 2.7 | 0.0 | 1.3 | -33.3 | 133.3 |
| AVERAGE | 35.7 | -37.7 | -44.0 | -56.2 | -40.2 |
| CCSM-driven | 70.4 | -48.3 | -55.6 | -75.7 | -66.7 |
| CGCM-driven | 46.9 | -40.2 | -50.7 | -66.7 | -55.6 |
| GFDL-driven | 12.0 | -37.6 | -41.0 | -43.8 | -91.7 |
| HADCM-driven | 2.7 | -18.3 | -21.3 | -30.0 | 100.0 |

TABLE 6. Question: Is the specific feature well enough represented such that it contributes to the credibility of the final precipitation projection? Y = Yes and N = No. The more "yes" answers, the more credible the simulation.

| | Specific Humidity | Monsoon Anti-cyclone | GoC LLJ | Easterly Waves | ENSO | Precipitation Intensity Bias | Other | "Other" Description | # of "Yes" Answers |
|---|---|---|---|---|---|---|---|---|---|
| **CRCM-ccsm** | N | N | Y | N | N | Y | Y | | 3 |
| **MM5I-ccsm** | N | N | N | N | N | Y | N | Drift | 1 |
| **WRFG-ccsm** | N | N | Y | N | N | Y | Y | | 3 |
| **CRCM-cgcm** | N | N | Y | Y | N | Y | Y | | 4 |
| **RCM3-cgcm** | N | N | N | Y | N | N | Y | | 2 |
| **WRFG-cgcm** | N | N | Y | Y | N | Y | Y | | 4 |
| **ECP2-gfdl** | Y | Y | N | N | Y | N | N | Excessive Late Summer/Fall Precipitation | 3 |
| **HRM3-gfdl** | Y | Y | Y | N | Y | Y | N | | 5 |
| **RCM3-gfdl** | Y | Y | N | N | Y | N | N | | 3 |
| **HRM3-hadcm** | Y | Y | Y | Y | Y | Y | Y | | 7 |
| **MM5I-hadcm** | Y | Y | N | Y | Y | Y | N | Drift | 5 |
| **# of "Yes" Answers** | 5 | 5 | 6 | 5 | 5 | 8 | 6 | | |

## LIST OF FIGURES

the color saturation and value (the vertical axis on the color bar). To facilitate creating this ensemble average, all models were regridded to a common 0.5° Õ 0.5° latitude/longitude grid.

3. JA average precipitation change (%) from the baseline period. Hatching indicates where the change is statistically significant at the 0.1 level.

4. Percent change from the current period to the future in the frequency of 3-hourly precipitation rates in JA for a) AZ and b) MX subregions. Rates are binned according to their percentiles in the baseline climate. The given number associated with a bin is the starting point for values within that bin; for example, the blue 90th percentile bin examines the change in the frequency of events with a magnitude greater than or equal to the 90th percentile magnitude and less than the 95th percentile magnitude from the current climate period. A dark block under a given bin at the bottom of each panel indicates that the change in that bin is statistically significant at the 0.1 level.

5. JA average precipitation change (%) from the baseline to the future period versus the precipitation bias (%). Bias is defined as the models' baseline period average (1971-1999) simulation minus NARR (1980-2003). Values are the average of land points only over the NAM "core" region. The linear fit applied to the points does not include the driving GCM results (open black symbols).

6. JA average change from the baseline to the future climate in the CCSM-driven simulations along the cross-section locations noted in fig. 1. Left) Winds parallel to the cross-section (vectors) and winds perpendicular to cross-section (color fill) across the GoC (cross-section from approximately west-to-east/left-to-right). Center) Winds parallel to the cross-section (vectors), temperature (red contours, every 0.5 ºC), and specific humidity (color fill) along the GoC (southern most point is to the left). Right) As for the center column, but for AZ (southwestern-most point to the left). Note that vertical velocity is multiplied by a factor of 1000 for visibility.

7. JA average location and strength of the 500-hPa geopotential monsoon anticyclone center in the baseline (filled circle) and future (open circle). The size of the filled and open circles represents the magnitude, following the key on the right. This includes NCEP, the filled grey circle in all panels, at 5931-m, the central circle size. Thin vectors indicate the baseline period speed and direction of the JA 500-hPa mean flow at select locations. Bold vectors attached to the tip of the baseline vectors indicate the change in flow from the baseline to future period (i.e., bold vectors are difference vectors, the future vector, if plotted, would start at the base of the historical vector and point to the tip of the difference vector). Some bold difference vectors are very small and barely visible, as there is very little change in the future flow from the baseline in some locations/simulations. Note that geopotential height is not available from the RCM3; therefore, the magnitude of the anticyclone center in this figure for RCM3 only is set to that of NCEP for the current and future, and the location of the center of maximum heights is taken as the center of the circulation in the 500-hPa wind field instead of as the

maximum in the 500-hPa geopotential height field. Also, except for the 500-hPa geopotential height field, no other upper-level information is available from the ECP2-gfdl at the time of writing; therefore, no wind vectors are plotted for this simulation.

8. CCSM and CCSM-driven RCMs JA 1971-1999 to 2041-2069 average change in 700-hPa wind speed and direction in m/s (1 m/s reference vector inset in panel d). Light grey shading indicates that the change is significant at the 0.1 level.

9. As in fig. 6, but for the CGCM-driven simulations.

10. Variance of 2-6 day band-pass filtered Eddy Kinetic Energy (EKE) at 700 hPa averaged over July-September from (a) NCEP (b), ERA-I, (c) CGCM, (d) CCSM, (e) GFDL, (f) HADCM. EKE is calculated from daily mean zonal and meridional winds. EKE is an estimation of African Easterly wave activity.

11. As in 8, but for the CGCM and CGCM-driven RCMs.

12. JA average change in precipitation intensity from the baseline to the future period versus the precipitation intensity bias (mm/day). Bias is defined as a model's current period average (1971-1999) minus NARR (1980-2003). Values in a) are the average over the NAM "core" region land points only. b) and c) are subregions as defined in fig. 1.

13. Hovmoller diagrams of daily precipitation (mm/day) from the RCM3-cgcm (higher precipitation intensity RCM) and CRCM-cgcm (lower precipitation intensity RCM) for an extreme dry year (1981, baseline; 2053, future) and wet year (1988, baseline; 2060, future) in the baseline and future simulations during June-August. Precipitation is averaged over 30ºN to 37.5ºN.

14. As in fig. 6, but for the HADCM-driven simulations.

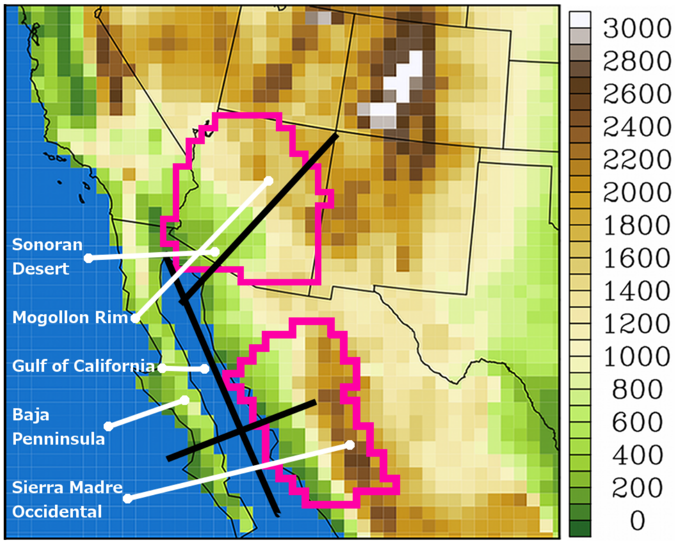


FIG. 1. Surface elevation (m) over land from the HRM3. Ocean points are filled in blue. Names and location indicators for important topographic features indicated with white text and lines. Outlines for analysis subregions, Arizona (AZ) and Northwest Mexico (MX), in magenta. Large NAM "core" region covers the full area shown. Locations for vertical cross sections along and across the Gulf of California and through AZ indicated in heavy black lines. Note that analysis subregions are not exactly identical between the different RCMs, as their projections vary. Grid points nearest given latitude/longitude coordinates for cross-section ends, box corners (for "core" region), or subregion mask points (for AZ and MX) are used. Also note that the southern extent of each RCM varies, and this impacts the size of the NAM "core" analysis region. Most NARCCAP RCM domains end around the southern tip of the Baja Peninsula.

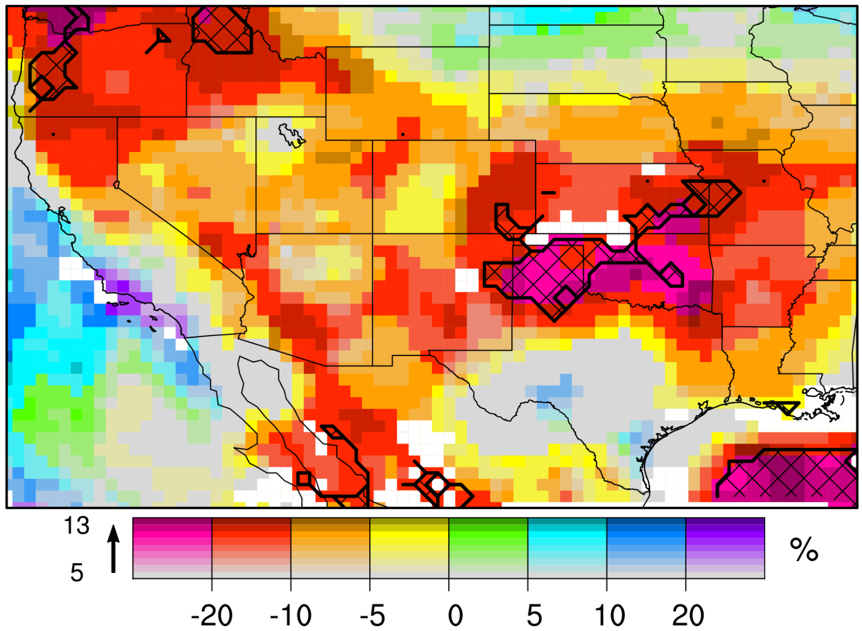


FIG. 2. Average JA precipitation change (%) from the baseline period in the 11-model ensemble mean. Precipitation is presented following methodology proposed by Tebaldi et al. (2011), with slight modification: hatching indicates where more than 50% of the models show change that is significant at the 0.10 level (as determined by a t-test) and where more than 75% of the models agree on the sign of change (thus, where the majority of the models agree on significance and sign). White grid cells indicate where more than 50% of the models show change that is significant but also where 75% of the models or less agree on the sign of the change (thus indicating true disagreement and little information). Additionally, the number of models that agree on the sign of the change is indicated by the color saturation and value (the vertical axis on the color bar). To facilitate creating this ensemble average, all models were regridded to a common 0.5° × 0.5° latitude/longitude grid.

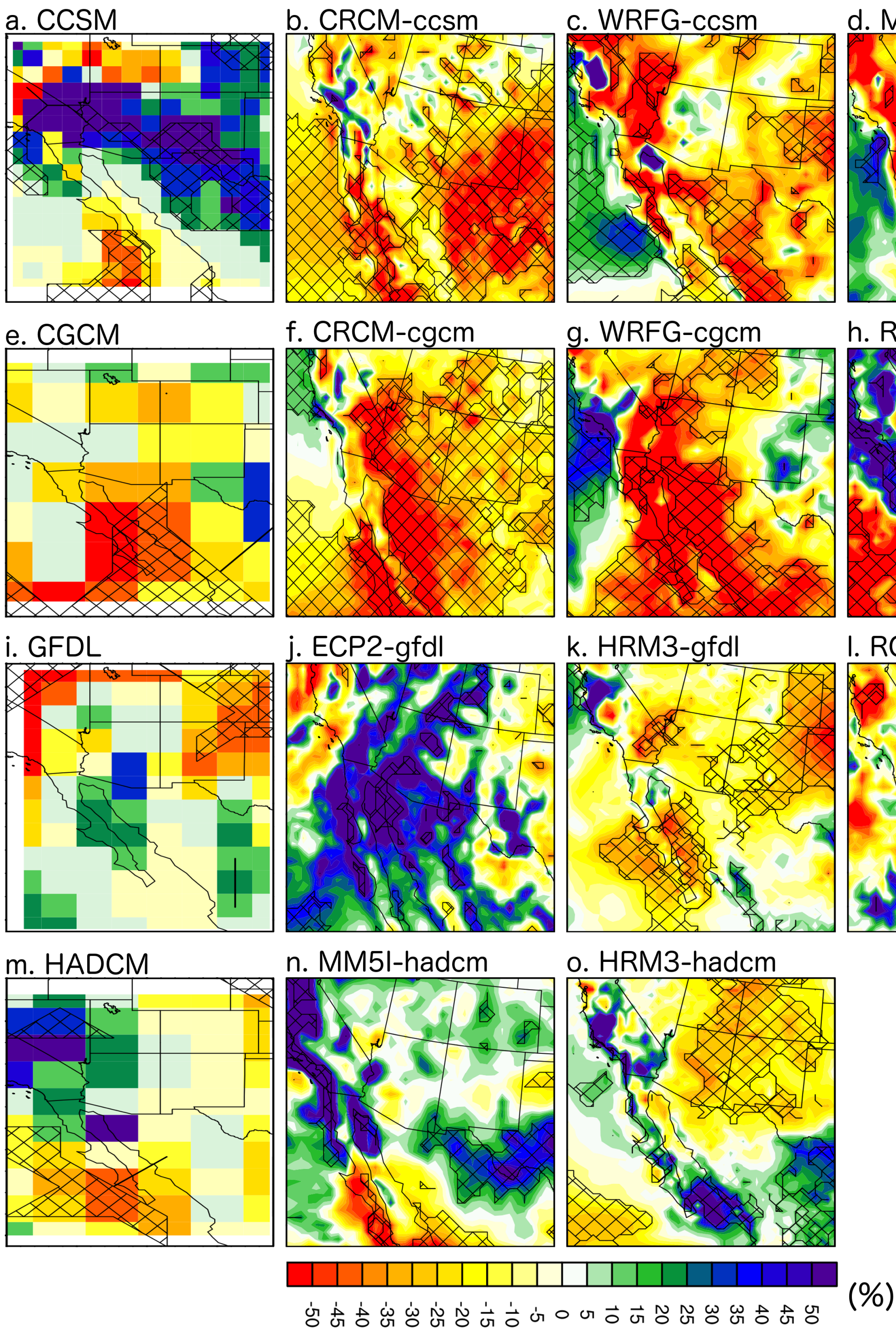


FIG. 3. JA average precipitation change (%) from the baseline period. Hatching indicates where the change is statis- tically significant at the 0.1 level.

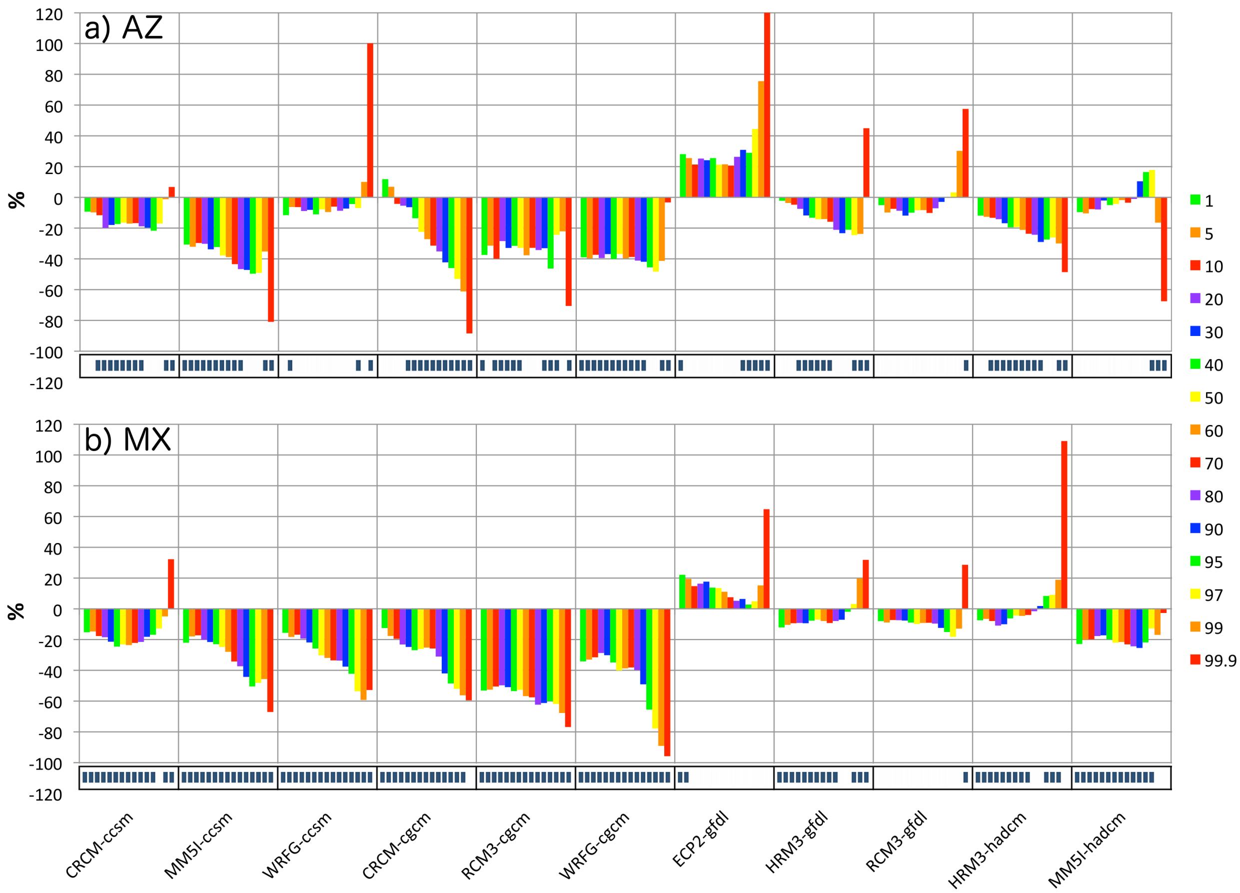


FIG. 4. Percent change from the current period to the future in the frequency of 3-hourly precipitation rates in JA for a) AZ and b) MX subregions. Rates are binned according to their percentiles in the baseline climate. The given number associated with a bin is the starting point for values within that bin; for example, the blue 90th percentile bin examines the change in the frequency of events with a magnitude greater than or equal to the 90th percentile magnitude and less than the 95th percentile magnitude from the current climate period. A dark block under a given bin at the bottom of each panel indicates that the change in that bin is statistically significant at the 0.1 level.

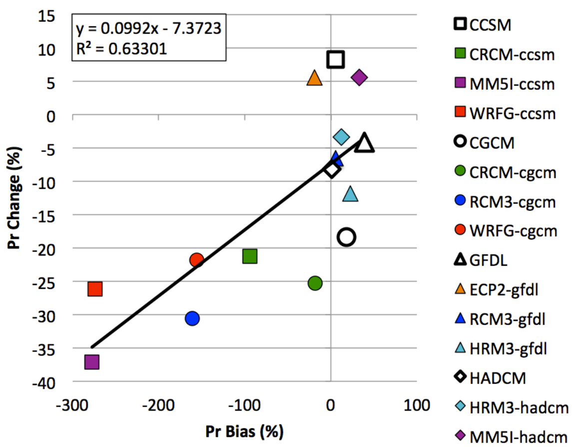


FIG. 5. JA average precipitation change (%) from the baseline to the future period versus the precipitation bias (%). Bias is defined as the models' baseline period average (1971-1999) simulation minus NARR (1980-2003). Values are the average of land points only over the NAM "core" region. The linear fit applied to the points does not include the driving GCM results (open black symbols).

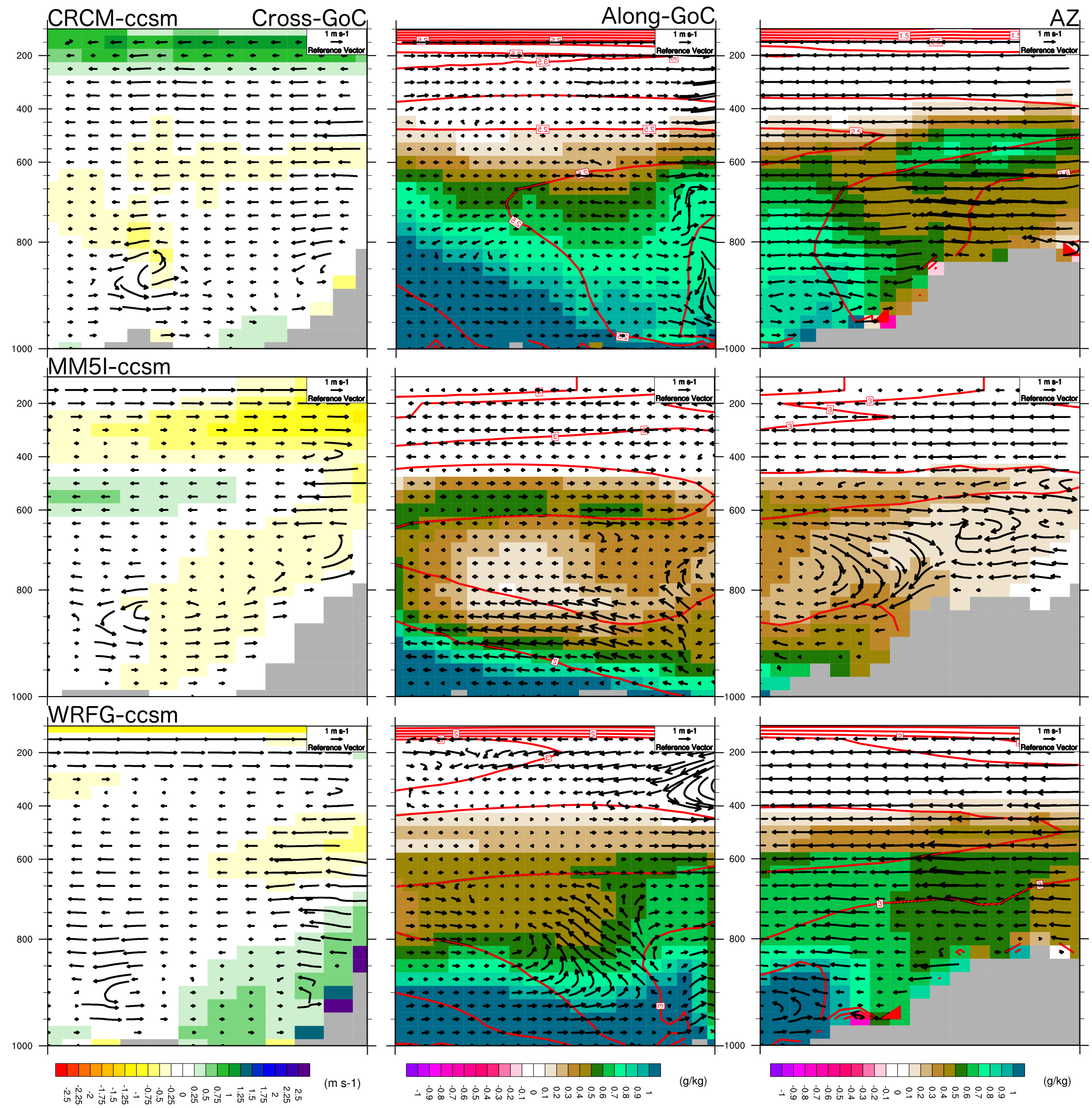


FIG. 6. JA average change from the baseline to the future climate in the CCSM-driven simulations along the cross- section locations noted in fig. 1. Left) Winds parallel to the cross-section (vectors) and winds perpendicular to cross-section (color fill) across the GoC (cross-section from approximately west-to-east/left-to-right). Center) Winds parallel to the cross-section (vectors), temperature (red contours, every 0.5 oC), and specific humidity (color fill) along the

GoC (southern most point is to the left). Right) As for the center column, but for AZ (southwestern-most point to the left). Note that vertical velocity is multiplied by a factor of 1000 for visibility.

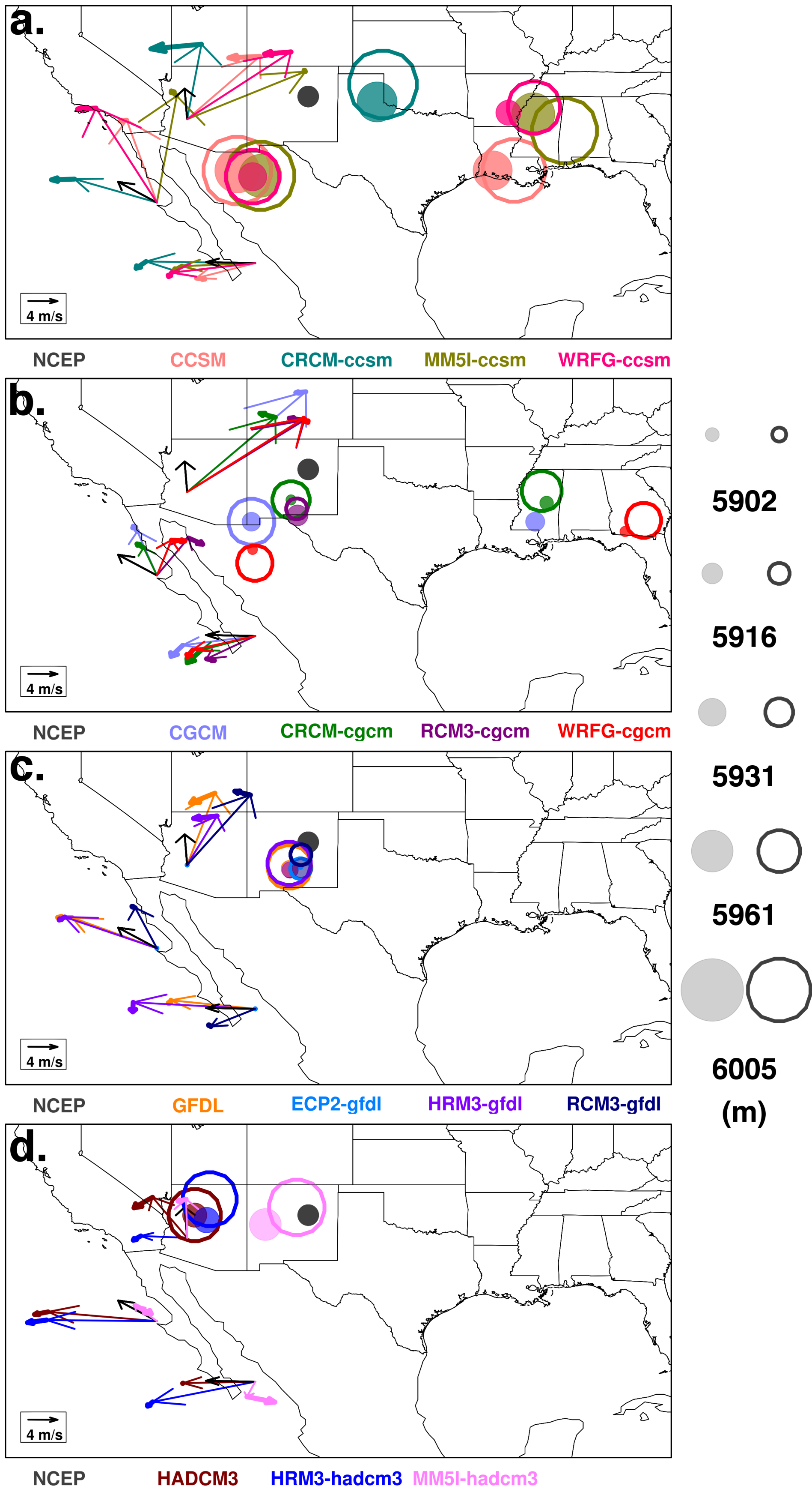
a.
4 m/s
NCEP
CCSM
CRCM-ccsm
MM5I-ccsm
WRFG-ccsm
b.
4 m/s
NCEP
CGCM
CRCM-cgcm
RCM3-cgcm
WRFG-cgcm
c.
4 m/s
NCEP
GFDL
ECP2-gfdl
HRM3-gfdl
RCM3-gfdl
d.
4 m/s
NCEP
HADCM3
HRM3-hadcm3
MM5I-hadcm3
5902
5916
5931
5961
6005
(m)

FIG. 7. JA average location and strength of the 500-hPa geopotential monsoon anticyclone center in the baseline (filled circle) and future (open circle). The size of the filled and open circles represents the magnitude, following the key on the right. This includes NCEP, the filled grey circle in all panels, at 5931-m, the central circle size. Thin vectors indicate the baseline period speed and direction of the JA 500-hPa mean flow at select locations. Bold vectors attached to the tip of the baseline vectors indicate the change in flow from the baseline to future period (i.e., bold vectors are difference vectors, the future vector, if plotted, would start at the base of the historical vector and point to the tip of the difference vector). Some bold difference vectors are very small and barely visible, as there is very little change in the future flow from the baseline in some locations/simulations. Note that geopotential height is not available from the RCM3; therefore, the magnitude of the anticyclone center in this figure for RCM3 only is set to that of NCEP for the current and future, and the location of the center of maximum heights is taken as the center of the circulation in the 500-hPa wind field instead of as the maximum in the 500-hPa geopotential height field. Also, except for the 500-hPa geopotential height field, no other upper-level information is available from the ECP2-gfdl at the time of writing; therefore, no wind vectors are plotted for this simulation.

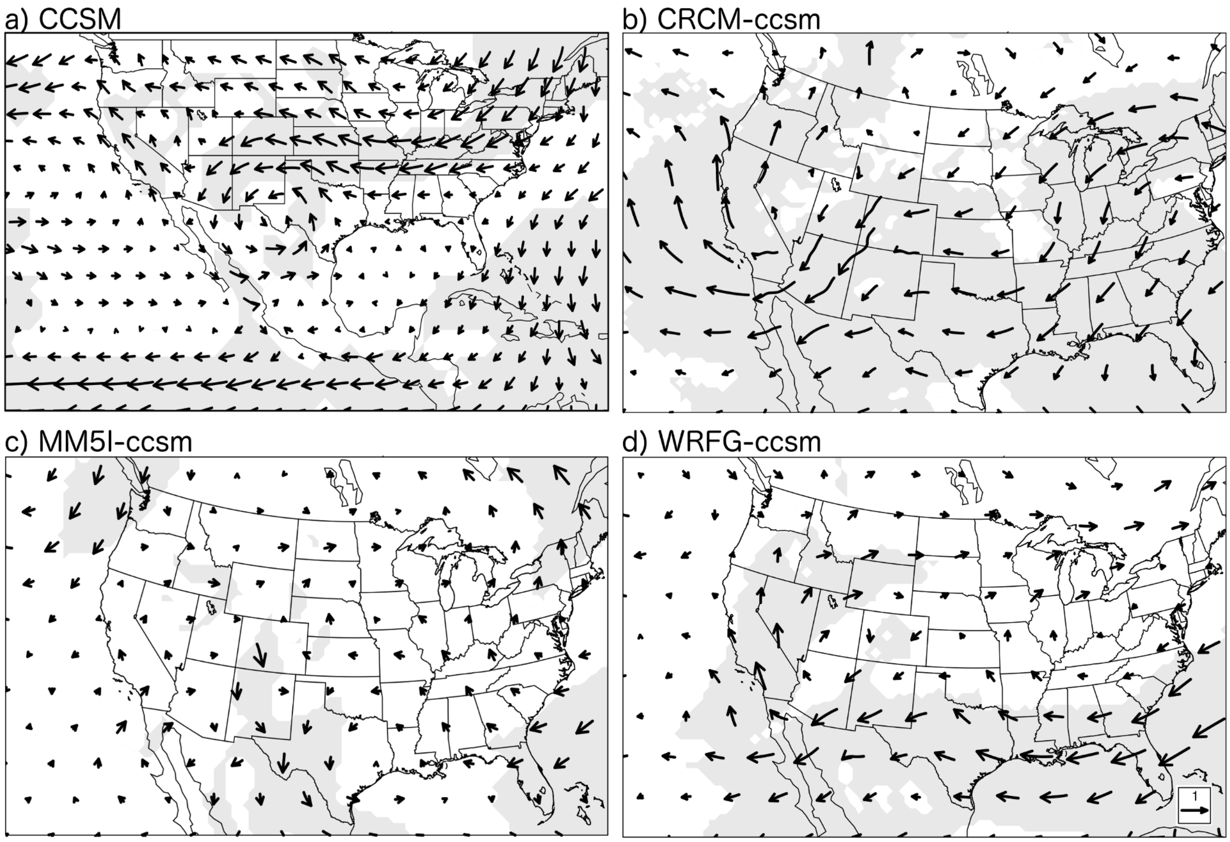


FIG. 8. CCSM and CCSM-driven RCMs JA 1971-1999 to 2041-2069 average change in 700-hPa wind speed and direction in m/s (1 m/s reference vector inset in panel d). Light grey shading indicates that the change is significant at the 0.1 level.

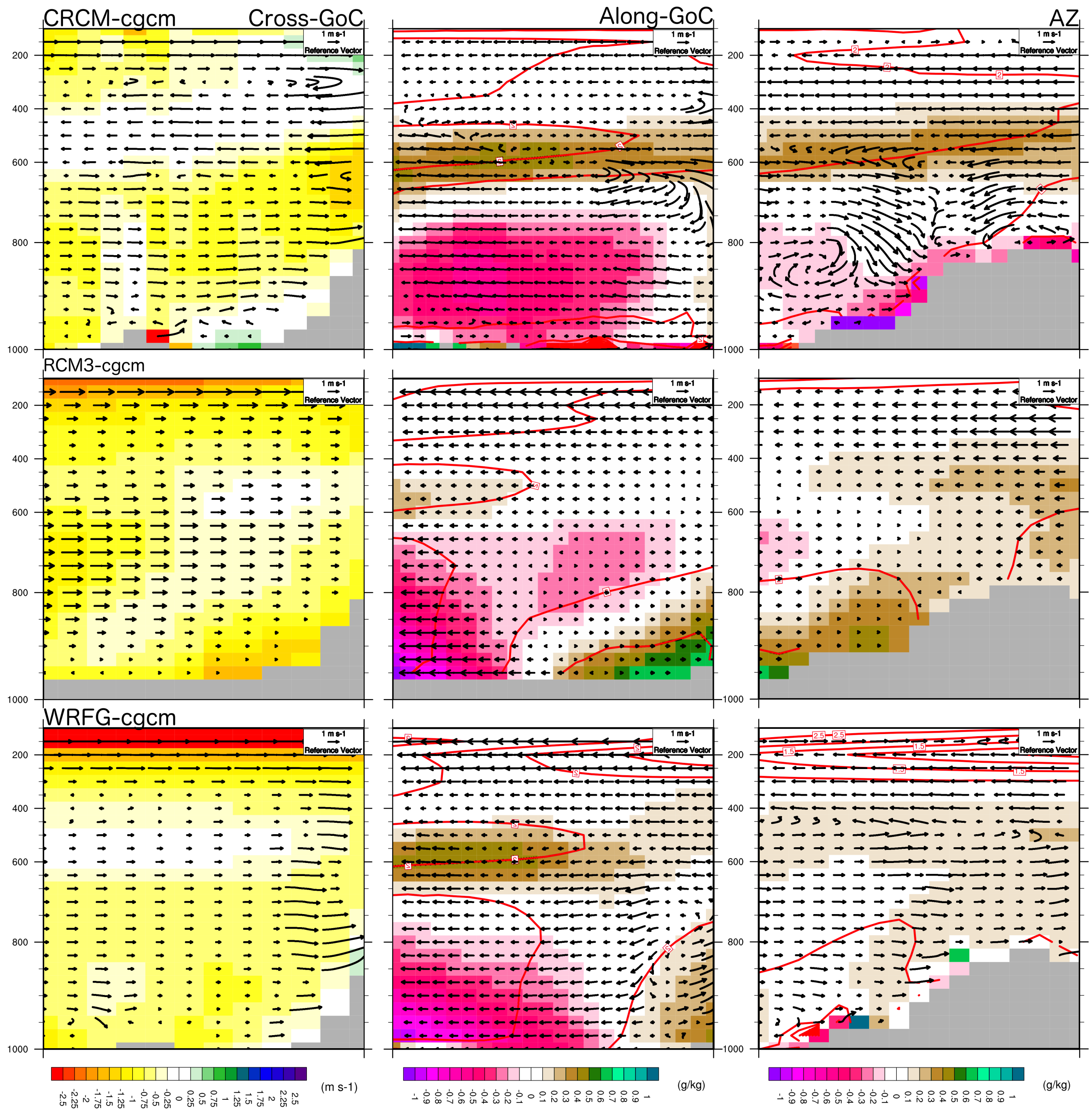


FIG. 9. As in fig. 6, but for the CGCM-driven simulations.

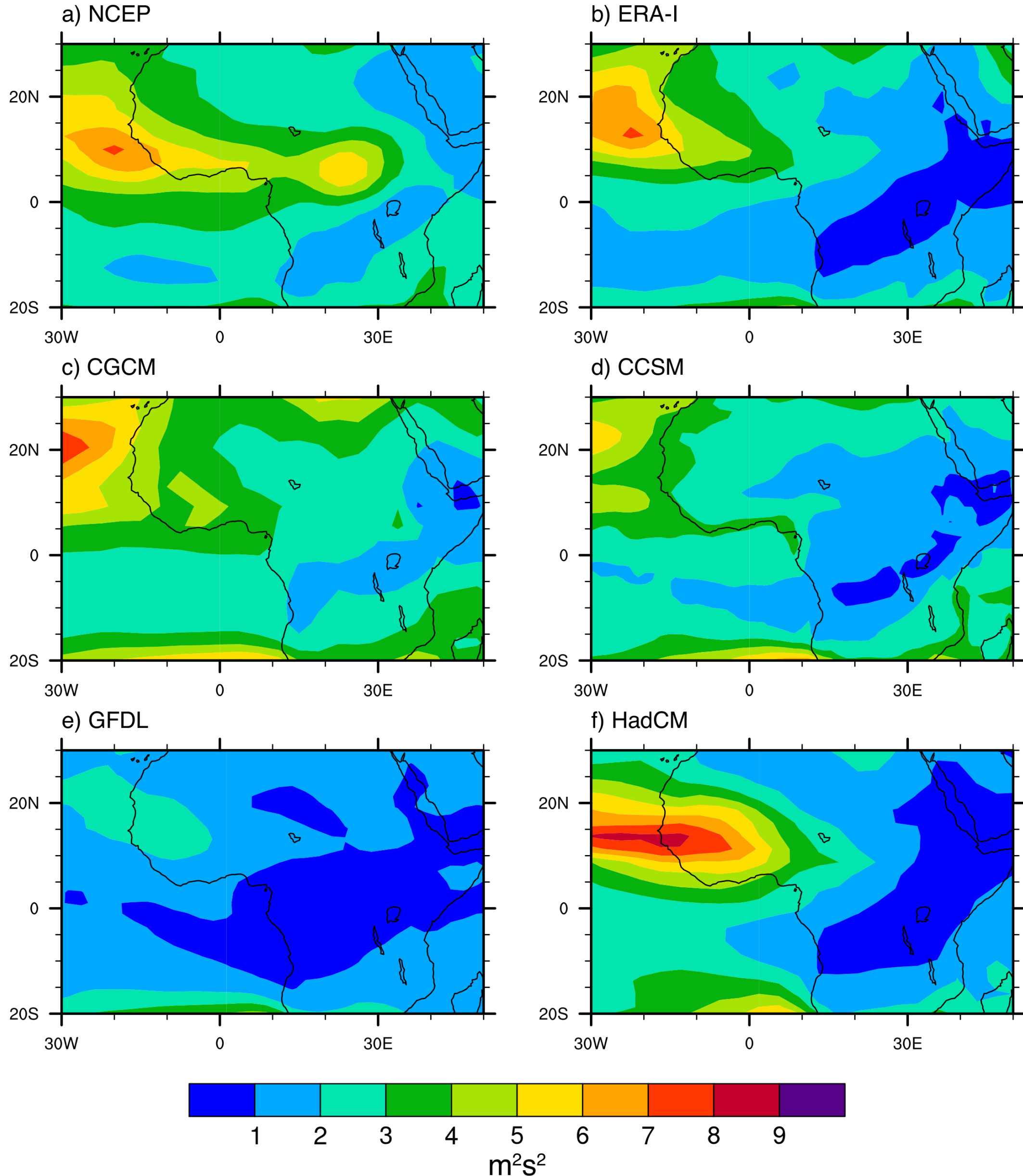


FIG. 10. Variance of 2-6 day band-pass filtered Eddy Kinetic Energy (EKE) at 700 hPa averaged over July-September from (a) NCEP (b), ERA-I, (c) CGCM, (d) CCSM, (e) GFDL, (f) HADCM. EKE is calculated from daily mean zonal and meridional winds. EKE is an estimation of African Easterly wave activity.

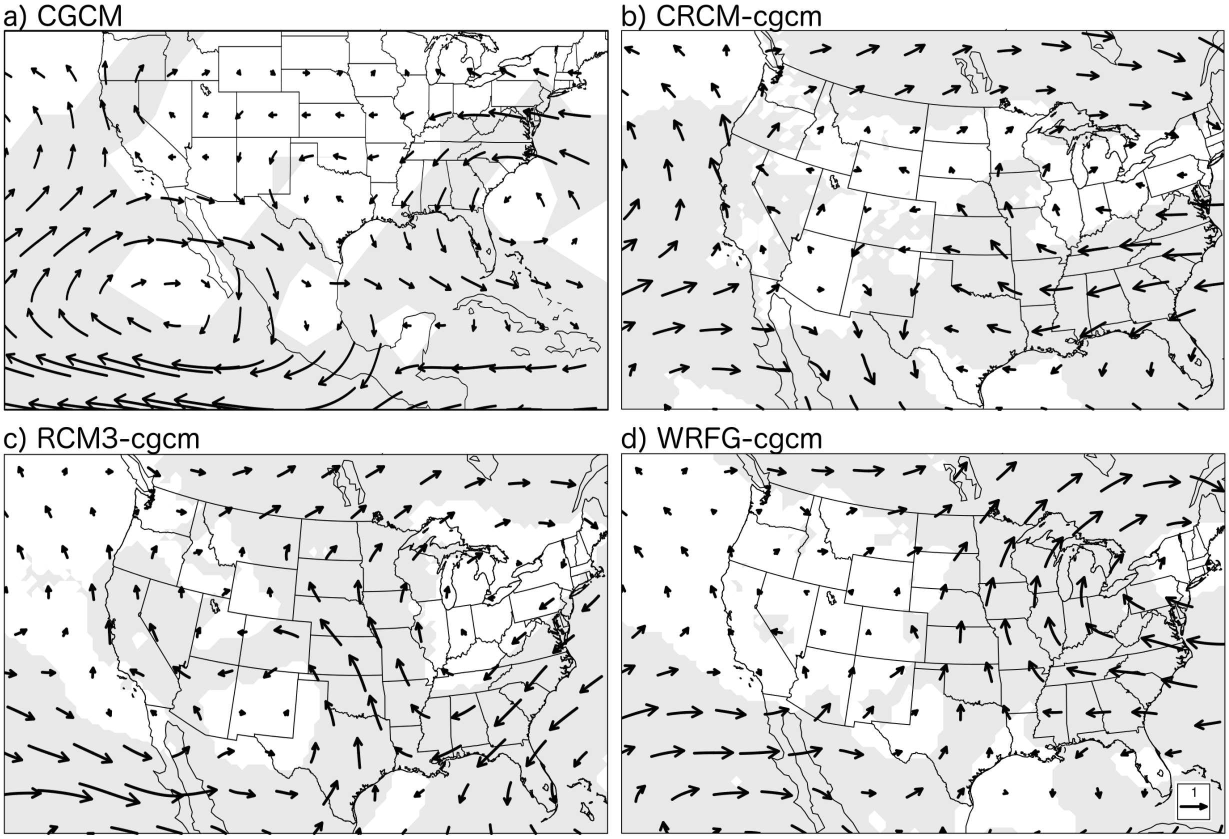


FIG. 11. As in 8, but for the CGCM and CGCM-driven RCMs.

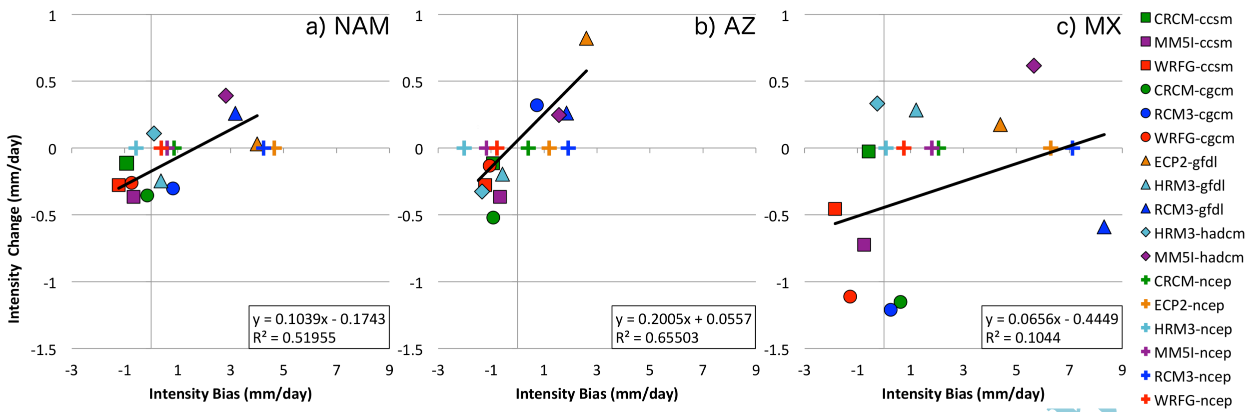


FIG. 12. JA average change in precipitation intensity from the baseline to the future period versus the precipitation intensity bias (mm/day). Bias is defined as a model's current period average (1971-1999) minus NARR (1980-2003). Values in a) are the average over the NAM "core" region land points only. b) and c) are subregions as defined in fig. 1.

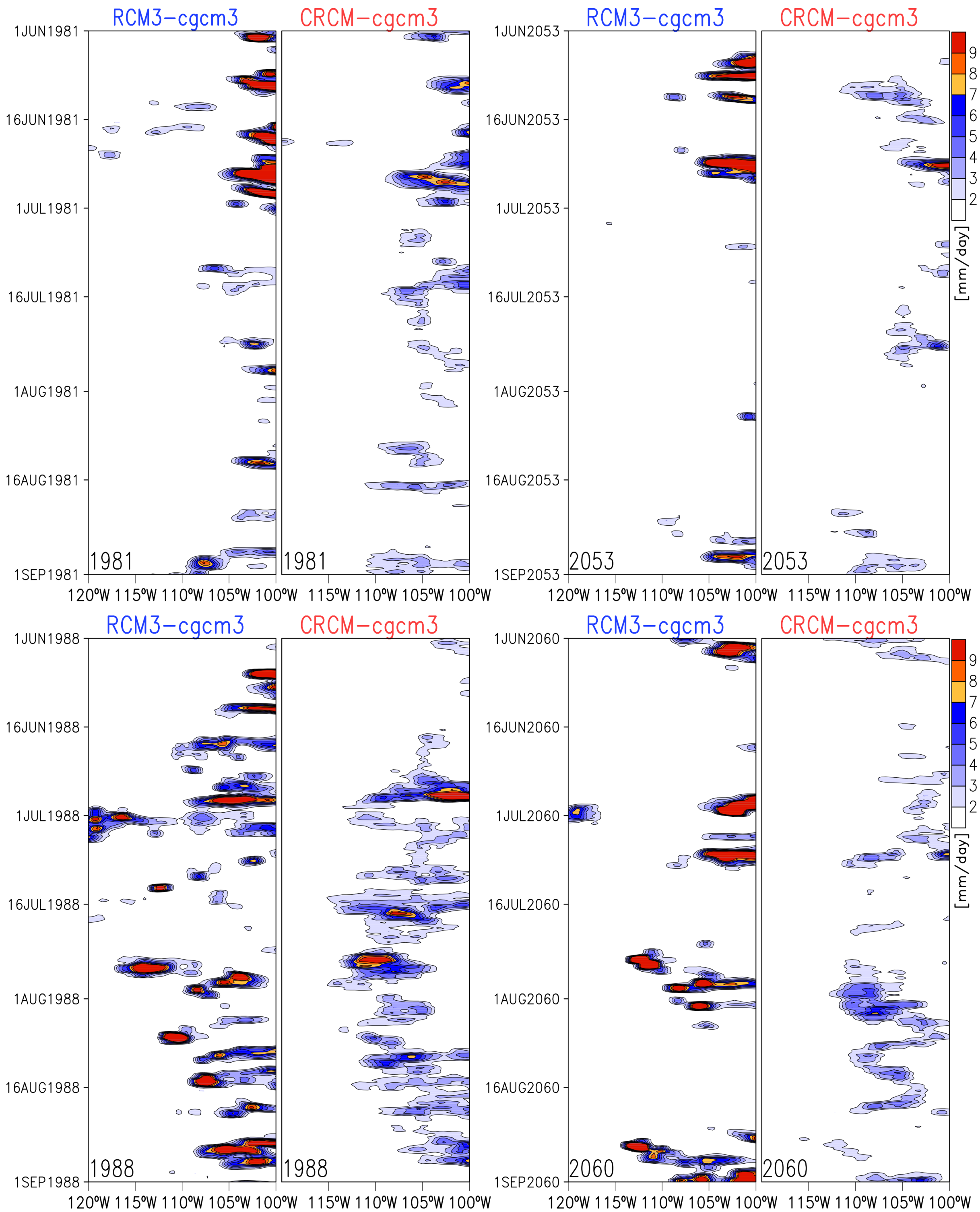
RCM3−cgcm3
CRCM−cgcm3
1JUN1981
16JUN1981
1JUL1981
16JUL1981
1AUG1981
16AUG1981
1SEP1981
1981
1JUN2053
16JUN2053
1JUL2053
16JUL2053
1AUG2053
16AUG2053
1SEP2053
2053
1JUN1988
16JUN1988
1JUL1988
16JUL1988
1AUG1988
16AUG1988
1SEP1988
1988
1JUN2060
16JUN2060
1JUL2060
16JUL2060
1AUG2060
16AUG2060
1SEP2060
2060
120°W 115°W 110°W 105°W 100°W
115°W 110°W 105°W 100°W
2 3 4 5 6 7 8 9
[mm/day]

FIG. 13. Hovmoller diagrams of daily precipitation (mm/day) from the RCM3-cgcm (higher precipitation intensity RCM) and CRCM-cgcm (lower precipitation intensity RCM) for an extreme dry year (1981, baseline; 2053, future) and wet year (1988, baseline; 2060, future) in the baseline and future simulations during June-August. Precipitation is averaged over 30oN to 37.5oN.

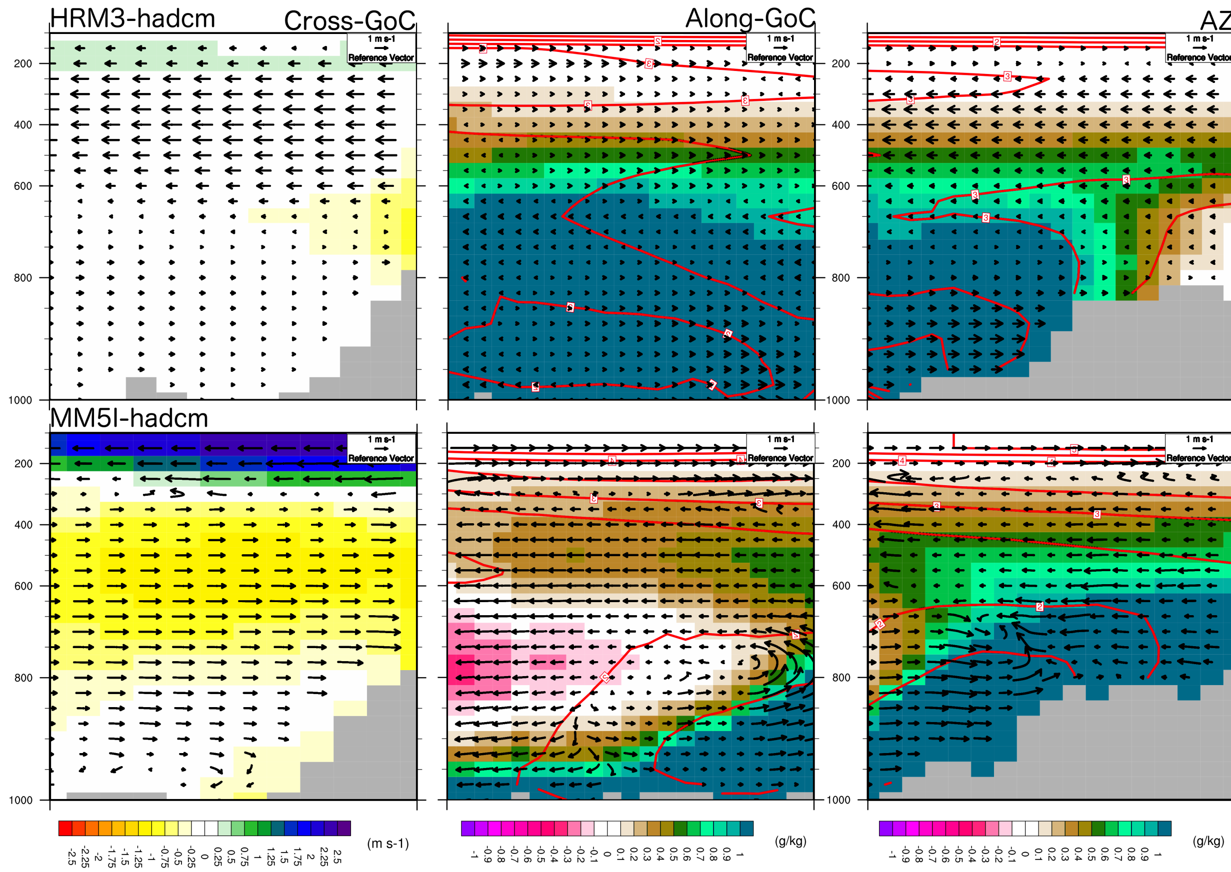


FIG. 14. As in fig. 6, but for the HADCM-driven simulations.